UNIVERSITY OF CALIFORNIA SAN DIEGO

Remodeling of Pulmonary Arteries During the Progression of Pulmonary Arterial Hypertension Using a Three Element Windkessel Model

A Thesis submitted in partial satisfaction of the requirements
for the degree Master of Science

in

Bioengineering

by

Sarita Giri

Committee in charge:

Professor Daniela Valdez-Jasso, Chair
Professor Xi Fang
Professor Andrew McCulloch

2022

The Thesis of Sarita Giri is approved, and it is acceptable in quality and form for publication on microfilm and electronically.

University of California San Diego

2022

DEDICATION

To

My mother, Gyanu
who taught me to believe in hard work and never give up on my dreams

My Father, Shyam
for earning an honest living and sacrificing your own needs to fulfill my dreams

My brother, Sishir
for constant support and encouragement

TABLE OF CONTENTS

LIST OF FIGURES

LIST OF TABLES

ACKNOWLEDGEMENTS

I would like to express my deepest gratitude to my professor Dr. Valdez Jasso for giving me the opportunity to be a part of her lab, my mentor Hao Mu for training me, Ethan Kwan for aiding me in data analysis and Bishal Mahat, Luyun Yang, Jessica Hubert, Yasser Abdelrahman, Kristen Garcia, Becky Hardie for the unlimited support and encouragement in everything I do. Finally, thank you Dr. McCulloch for your guidance, wisdom, and compassion.

VITA

2021 Bachelor of Science in Bioengineering, University of California San Diego

2022 Master of Science in Bioengineering, University of California San Diego

ABSTRACT OF THE THESIS

Remodeling of Pulmonary Arteries During the Progression of Pulmonary Arterial Hypertension Using a Three-Element Windkessel Model

by

Sarita Giri

Master of Science in Bioengineering

University of California San Diego, 2022

Professor Daniela Valdez Jasso, Chair

Pulmonary arterial hypertension (PAH) is a progressive disease characterized by an elevated mean pulmonary arterial pressure leading to right ventricular hypertrophy and failure. PAH is also associated with an increase in pulmonary vasculature resistance (PVR) due to the accumulation and proliferation of smooth muscle and endothelial cells in the intimal layer of the distal pulmonary arteries. This causes remodeling of the pulmonary vasculature, similar to the plexiform like lesions seen on the autopsy of PAH patients. Many studies have investigated the

microstructural and mechanobiological properties of the pulmonary arteries however, the main cause initiating this remodeling process still remains unknown. In this thesis, the remodeling of pulmonary arteries that causes the changes in the resistance and compliance properties of pulmonary vasculature as PAH progresses overtime was studied, using three different Sugen Hypoxia treated rat models (male, female, ovariectomized female) of PAH. A lumped three-element Windkessel model was used to reproduce the *in vivo* measured blood pressure data efficiently by estimating the resistance and compliance parameters. The parameters estimated by the three-element Windkessel model exhibited statistically significant differences and reflected the relevant physiological changes as the disease progressed. For example, our model revealed that the resistance and compliance changes during PAH, and that the resistance significantly increases ($p < 0.05$) only in male however the compliance significantly decreases ($p < 0.05$) in all three groups of rats. Also, the remodeling was sex specific because the compliance changes significantly and early in all three groups of rats before any major changes in the resistances for female and ovariectomized females (OVX) were observed. On the other hand, no statistically significant differences in the parameters and pressures were found between the female and OVX rats. Future direction for this study includes the development of one-dimensional fluid dynamic model to better understand the sex specific remodeling and compare these changes to the structural and tissue-level changes of biomechanical properties in the pulmonary arteries of male, female and OVX female rats. Such insights can potentially help improve our understanding of treatment therapies in either sex of PAH patients in future.

1. Background and Significance

1.1. Pulmonary Arterial Hypertension

Pulmonary arterial hypertension (PAH) is a progressive disease characterized by remodeling of pulmonary arteries and right ventricular hypertrophy. The complex nature of this disease causes an increase in pulmonary arterial pressure which leads to right ventricular dysfunction and failure. Clinically, PAH is defined as a resting mean pulmonary arterial pressure (mPAP) of 20mmHg or above and diagnosed using a right heart catheterization [1]. Patients with PAH are diagnosed at advanced stages because their symptoms in the early stages are usually mild and nonspecific. Symptoms such as shortness of breath, dizziness and chest pain will elevate overtime and patients will require immediate medical attention. There is currently no readily available cure for PAH with a poor prognosis of only 3-5 years [2]. Therefore, there is an urgent need to identify the pathophysiological changes in the pulmonary vasculature system that allows for the initiation and progression of PAH in patients.

1.2. Remodeling of Pulmonary Vasculature During PAH

Pulmonary arteries in PAH are impaired due to vasoconstriction and remodeling. Structural remodeling of the pulmonary arteries includes uncontrolled accumulation and proliferation of different vascular and inflammatory cells in the arterial wall [3]. This causes vascular fibrosis and gradual stiffening of the pulmonary vasculature. Studies have shown that nearly 15% of the PAH patients develop plexiform like vascular lesions in their pulmonary arteries which is an important

hallmark of the idiopathic pulmonary arterial hypertension [4, 5]. An increase in vascular obstructions causes pulmonary vascular resistance (PVR) to increase simultaneously with the increase in mPAP. Clinical guidelines suggest that the PVR is usually greater than 3 mmHg.min/l in PAH patients [6, 7]. Although changes in hemodynamic measurements- mPAP and PVR - can be used to diagnose PAH, studies have highlighted the importance of pulmonary arterial compliance that significantly drops during the early stages of PAH [8]–[10]. The significant decrease in the compliance is closely associated with the increase in matrix/collagen deposition in the pulmonary arteries hence stiffening the arteries [9, 11]. As the elastin content decreases, the compliance changes early, and even when the mPAP and PVR is normal in patients [8]. Additionally, several important genetic pathways (endothelin-1, prostacyclin, nitric oxide) have also been identified that contribute to the remodeling of the pulmonary arteries during the development and progression of PAH [12]–[15]. Given that the remodeling causes pulmonary arteries to stiffen during PAH, the main cause for this remodeling remains unknown.

Additionally, recent literatures have now started to focus on the influence of sex in PAH. PAH has been shown to develop at a higher frequency in females than in males. Several potential hypotheses have also been proposed that includes the role of estrogen and environmental exposure that put females at a higher risk for developing PAH than males [16]–[18]. Therefore, in our study we incorporated three different groups of rats – male, female and ovariectomized – and investigated how the resistance and compliance properties of pulmonary arteries change as PAH progresses overtime. Hence, it is critical to understand the changes in hemodynamic parameters like pulmonary arterial compliance and PVR as the vasculature remodels for the early diagnosis and treatment of PAH.

1.3. Constitutive Model of the Arterial System

Various computational models have been proposed to capture the hemodynamic changes in the arterial system. While lumped models like Windkessel [19]–[21] and T-tube [22], [23] uses electrical elements to characterize the compliant and resistive properties of a large vessel, distributed models [10], [24] uses different level of spatial interaction to assess the spatially-distributed phenomenon of the arterial system. For our study, we will be focusing on the Windkessel model. The idea of Windkessel model was first introduced by the German, physiologist Otto Frank [19]. He describes the arterial system of our body as a closed circuit that consists of a pump connected to an air-chamber which he calls Windkessel. Briefly, the Windkessel is a simple mathematical model used to describe the dynamics of an arterial system using electrical parameter such as a resistor and capacitor. Although these parameters are commonly interpreted in an electrical system, a direct analogy exist that relates an electrical circuit to a fluid system. For example, the relationship between fluid pressure and volume related by resistance $P = QR$, is parallel to the governing equation that defines an electrical system $V = IR$ [21]. Therefore, a lumped or Windkessel model with electrical elements like a resistor and a capacitor can be used to understand the changes in resistance and compliance properties of a systemic or pulmonic arterial system. The variants of Windkessel model vary depending on the number of electrical elements added to it. Figure 1.3 shows the concept of Windkessel model that is used to accurately resemble the mechanics of our heart.

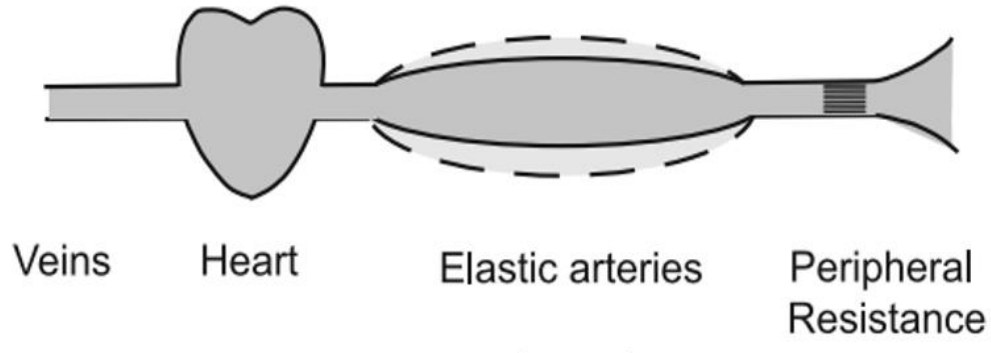

Figure 1.1: Diagram showing the concept used to describe the Windkessel model used by Otto Frank. The Windkessel chamber acts like a large elastic arterial vessel in our body. Image adapted from Westerhof et al. Medical & Biological Engineering & Computing 2009.

Moreover, many studies have suggested using Windkessel model to understand the hemodynamic changes in the pulmonary arteries. A lot of them have used a three-element Windkessel model to estimate changes in the resistance and compliant properties of a pulmonary vessels during PAH [25]–[27]. Although several variants of Windkessel models are established, a three element Windkessel model was found to be robust and sufficient to estimate these changes in pulmonary vasculature [9], [20], [27], [28]. Hence, the objective of this study is to understand the hemodynamic changes in the pulmonary vasculature using a three-element Windkessel model in different groups of sugen-hypoxia (SuHx) treated rats.

1.4. Specific Aims

The goal of this study is to understand the changes in pulmonary vasculature during the progression of PAH in different groups of rats. To study the changes in pulmonary vasculature represented by the changes in a resistance and compliance, we will use a three-element Windkessel model.

Aim 1: Investigate the resistance and compliance properties of PA during PAH.

We hypothesize that the resistance and compliance properties of pulmonary arteries change during PAH. To test our hypothesis, we will use a three-element Windkessel model and asses these changes in pulmonary vasculature as PAH progress overtime.

Aim 2: Distinguish the changes in pulmonary vascular properties in male and female rats, and how sex hormones contribute to these changes in female animals.

Because PAH is more prominent in females than in males, we hypothesize that the changes in resistance and compliance properties of a pulmonary vasculature is sex specific and that the sex hormone – estrogen may not be regulating these changes. To test this hypothesis, we will incorporate SuHx treated male and female rats to study the changes in pulmonary vasculature properties. We will also use OVX female rats and compare these changes to the female rats in order to understand the role of estrogen using a lumped three-element Windkessel model.

2. Methods

In this Chapter, we narrate how sugen hypoxia (SuHx) is induced in an animal model of pulmonary arterial hypertension, how we take the *in vivo* hemodynamic measurements from these animals and interpret the measurements using constitutive model.

2.1. Animal Model of PAH: Experimental Design

We use SuHx Sprague-Dawley rat models to study the progression of PAH. Male weighing $\sim 200g$ at 6 weeks of age, female weighing $\sim 180g$ at 7 weeks of age, and OVX female rats weighing about ~200g were injected subcutaneously with a single dose of 20mg/kg of Sugen (SU5416, Sigma-Aldrich, St. Louis, MO) and kept in hypoxic chamber supplied with 10% oxygen for three weeks. OVX female rats for this study were ovariectomized by The Charles River Institutional Animal care and Use Committee (IACUC) and was shipped to us 7-10 days after the procedure. Sugen combined with chronic hypoxia was chosen because it develops plexiform like lesions similar to the one seen on the autopsy of the patients with PAH [29]. Sugen is a vascular endothelial growth factor receptor 2 (VEGFR-2) inhibitor. Normally, when the pulmonary arterioles constrict in response to hypoxia, VEGFR-2 receptor gets activated, to supports the maintenance, differentiation, and proper function of endothelial cells [30]. However, when VEGFR-2 receptor is inhibited with sugen, endothelial cells start to accumulate in the pulmonary vessels hence increasing the pulmonary arterial pressure and right ventricular dysfunction [30], [31]. Thus, PAH continues to develop in these animals even when kept in normoxia after three weeks.

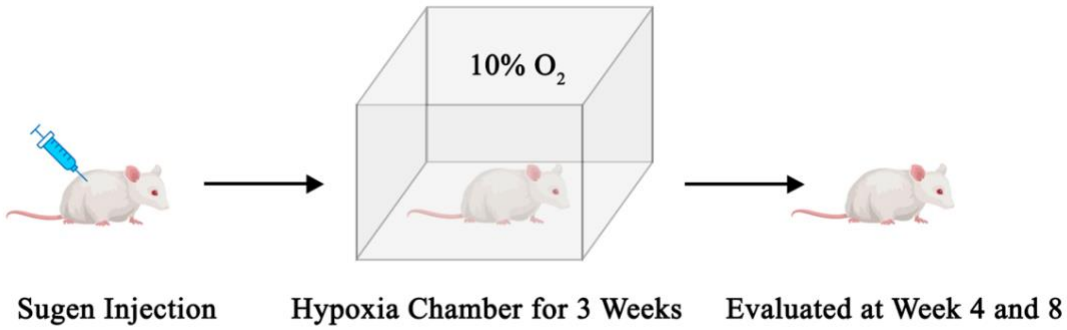

Figure 2.1: Schematic showing the experimental design of inducing PAH in Sprague-Dawley rats injected with sugen 5416 and hypoxia for three weeks and evaluated at week 4 and 8 for this study.

2.2. Data Acquisition: Surgery – Tracheotomy and Thoracotomy

After three weeks of continuous hypoxia exposure, the rats were returned to normoxia (20.9% O_2). An *in-vivo* hemodynamic measurements were taken by performing an open-chest surgery to obtain pulmonary arterial pressure and flow, at mPAP greater than 20 *mmHg*.

Before starting the surgical procedure, rats were placed into a chamber and supplied with 5% isoflurane mixed with oxygen as an anesthetic. Immediately after the rats fell asleep, they were transferred to the surgical platform with a nose cone attached to their nose exposing them to 2.5% isoflurane and oxygen. Tracheotomy procedure was performed on these animals by making a blunt incision vertically until the trachea was exposed while avoiding bleeding and cutting into the carotid arteries. The trachea was isolated, and a suture was placed behind it to secure the intubation (E-Z Anesthesia Ventilation system, Palmer, PA). The ventilator pressure and their heart rate were closely monitored and noted between 2-8 cmH_2O and 280-320 beats per minute (BPM). Following

tracheotomy, thoracotomy was performed where these animals underwent an open-chest surgery to obtain an *in-vivo* hemodynamic measurements using different catheters and probes.

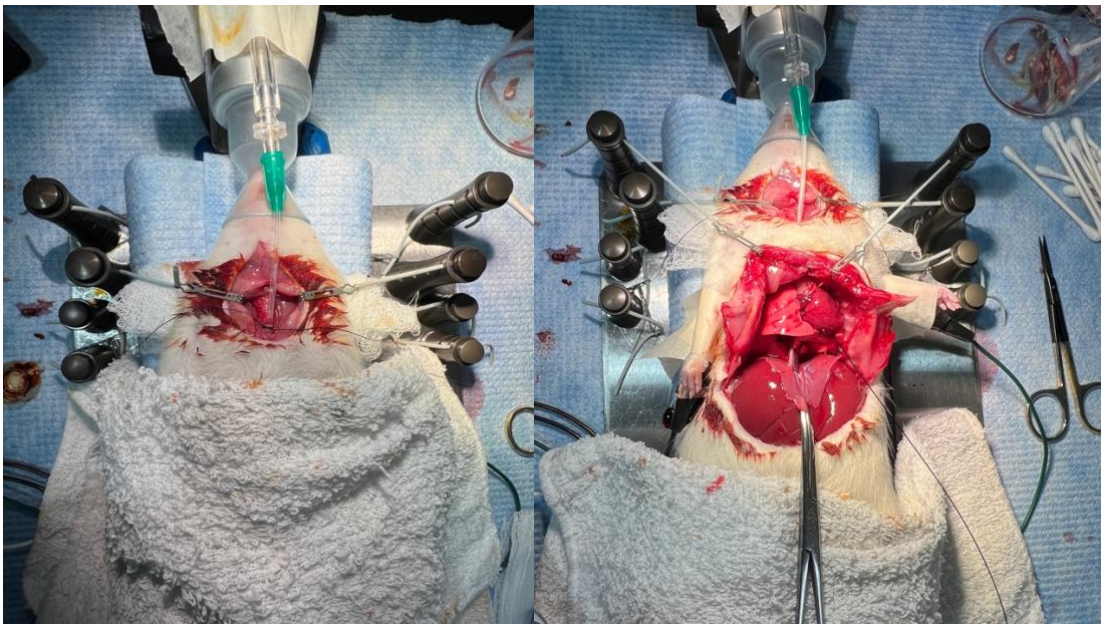

Figure 2.2: Data acquisition by performing tracheotomy (left) and thoracotomy (right) surgery in SuHx induced PAH rats.

An incision was made below the sternum across the abdomen so the heart could be exposed, and pressure-volume measurements can be taken. Initially, a 1.9-F 6.0mm pressure-volume (PV) catheter (Transonic Science, London, ON, Canada) was inserted into the right ventricle of the heart to get the pressure and the instantaneous volume measurements. Similarly, a 1.6F (Transonic Science, London, ON, Canada) Dual pressure (DP) catheter was then inserted into the right ventricle and advanced to the main pulmonary artery via pulmonary valve to obtain both the right ventricular and pulmonary arterial pressure in a time series. The heart rate after the catheter insertion was closely monitored by ECG and heart rate signal in the monitor. It was noted that the female rats generally tend to have a higher heart rate (340-360 BPM) than males (270-320 BPM). Additionally, a TS420 flow modulus and compatible flow probe (PMP-series 2-14 mm transonic

ultrasonic transit-time technology) was used to measure the absolute blood flow in the aorta and pulmonary artery.

2.3. *In vivo* Hemodynamic Measurements Using PV and DP Catheters

There are various techniques used to measure the hemodynamic parameters in cardiovascular research. Some of these well-established cardiac pressure-volume measurements techniques include echocardiography, pressure-volume catheterization, computer tomography (CT) and cardiac magnetic resonance (CMR) [32]. For hemodynamic measurements in our study, we used Pressure-Volume (PV), Dual Pressure-Volume (DP) catheters and ultrasound time-transit flow probe.

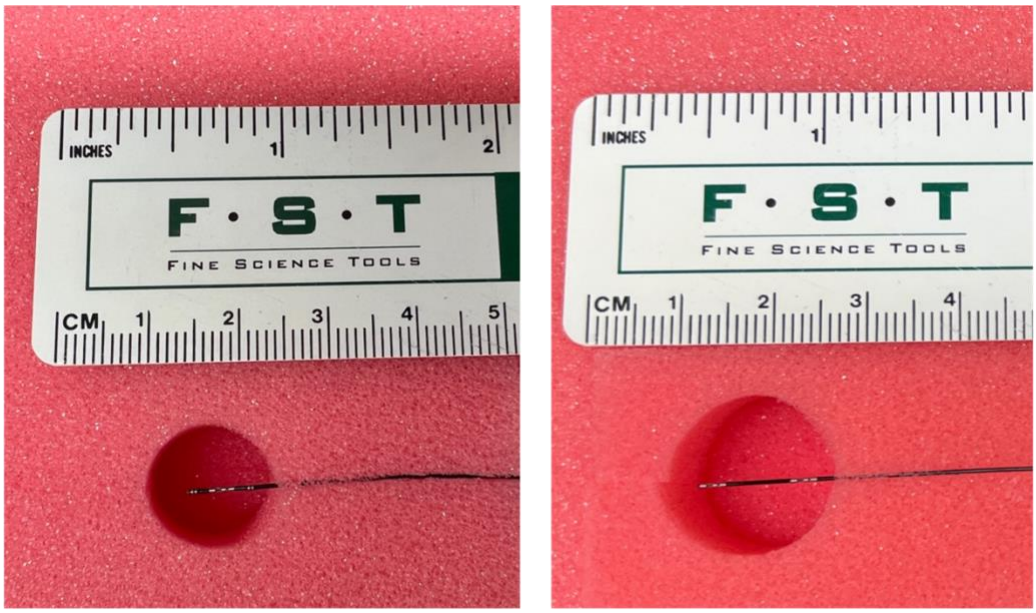

Figure 2.3: PV catheter (left) and DP catheter (right)

After the insertion of PV catheter into the right ventricle, real-time pressure and volume measurements are acquired. In short, our PV and catheters have piezoresistive strain gauges built

in it that detects pressure through a flexible rubber membrane. This rubber membrane has a thin circuit printed on it and as the catheter experiences pressure, the membrane and the circuit deform causing the changes in the resistance which is detected by the Wheatstone bridge [33].

For the volume measurement in the right ventricle using PV catheter an admittance theory is used. Both PV and DP catheter consisted of both excitation and recording electrodes at the proximal and distal end. The excitation electrodes at both the proximal and distal end generate an electrical field as a result of an alternating current being applied between the two outermost electrodes inside the heart. The two innermost electrodes also known as the recording electrodes measure the voltage changes which therefore allows us to calculate the resistance and conductance using Ohm's law.

Figure 2.4: PV catheter inserted from the apex of the heart into the right ventricle. The two excitation electrodes on the catheter creates an electrical field and the two sensing electrodes senses the voltage change. Image adapted from Gerringer et al. Windkessel Models of PAH 2018.

The electrical field generated by the excitation electrodes consist of both muscles and blood. Blood and muscle response to alternating current very differently. While blood is purely resistive, the myocardium muscle of the heart has both capacitive and resistive properties. During

systole, as the ventricle contracts, there is a less amount of blood in the myocardium and as result the electric field generated mostly surrounds the myocardium of the heart (Figure 2.5). However, during diastole, there is a large quality of the blood in the ventricle as the heart relaxes and the electrical fields mostly pass through the blood with a very small contribution of the myocardium walls [33]. Note that figure 2.5 shows the electrical field generated by the catheter on left ventricle unlike the catheter which are inserted from the apex of the heart to the right ventricle during our surgeries.

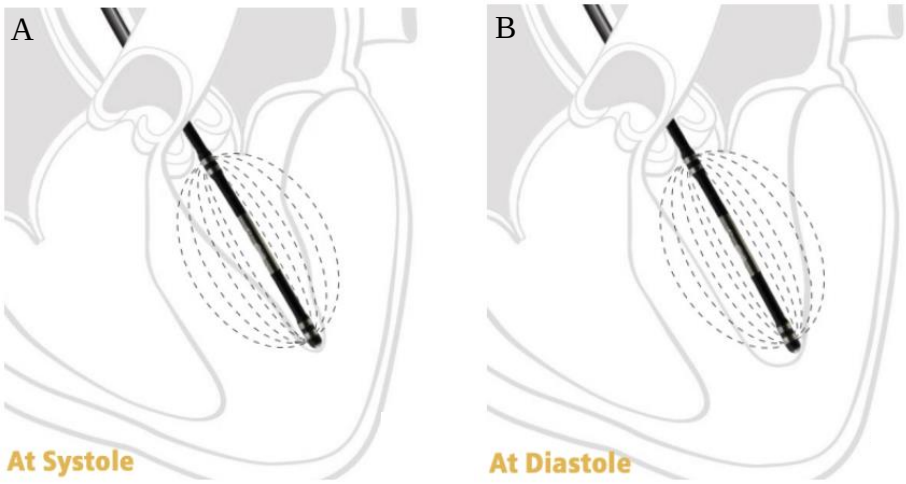

Figure 2.5: Electrical fields generated by the excitation sensing sensor during systole and diastole. (A) During systole, the electrical field consists of a large number of myocardial walls and less blood. (B) During diastole, the electrical field consists of a large amount of blood volume and less myocardial wall. Image adapted from Transonic PV workbook RPV-wb Rev D 2019.

The changes in voltage measured by two inner recording electrodes in the catheter is related to the conductance by Ohm's law $V = IR$. Conductance simply is the reciprocal of the resistance. During systole, when the electrical field mostly penetrates through the myocardium, it gives rise to an additional conductance also known as a parallel or muscle conductance [33]. The muscle conductance must be removed from the total conductance measurement which is why admittance

mode is used for the real-time volume measurement in our experiment [6]. Because the muscle cells have both resistive and capacitive properties with fixed charges, they create a significant delay in the phase (time) signal that causes a phase shift between the measured signal and the excitation signal [33].

Admittance theory uses this phase shift between the two signals to determine the instantaneous muscle conductance which is thereafter removed from the total measured conductance. The conversation of the total measured conductance into the volume is done using Wei's Equation [33] below:

$$Vol = \frac{1}{1-\frac{G_b}{\gamma}} \rho L^2 \, (G_b) \tag{2.1}$$

Here, ρ is the blood resistivity, L is measuring electrode distance and G_b is the measured blood conductance.

In addition to the pressure and volume, we also get to read phase signals in the Lab Chart software. Phase signal is usually periodic in shape and helps us to visualize distance between the catheter and cardiac wall. Phase signal greater than four means high proximity of the catheter to the heart wall, thus suggests a better catheter placement. Magnitude on the other hand is generally the amount of blood flow or the measurement of blood conductance measured by the catheter. It is typically measured to be around 1400-2600 micro siemens μS in healthy rats.

2.4. Hemodynamic Measurement Using Flow Probe

In order to measure the volume flow as a cardiac output, an ultrasound flow probe (Transonic Scisense, Ontario, Canada) was wrapped around the main pulmonary artery and aorta.

Our flow probe is made up of two ultrasonic transducers that emit the sound rays to form an ultrasonic beam into the bloodstream. As the blood is flowing through the arteries, they reflect these ultrasonic beams which as a result shifts the frequency of the beam received by the second transducer on the probe. The shift of frequency or the phase shift in transit time is proportional to the average velocity of the blood flowing through the arteries [34] . The receiving transducers therefore integrate this velocity over the vessel's width yielding volume flow in transit time or the cardiac output in the Lab Chart software. Figure 2.6 shows the working mechanisms of a flow probe used in our study to measure cardiac output in rats.

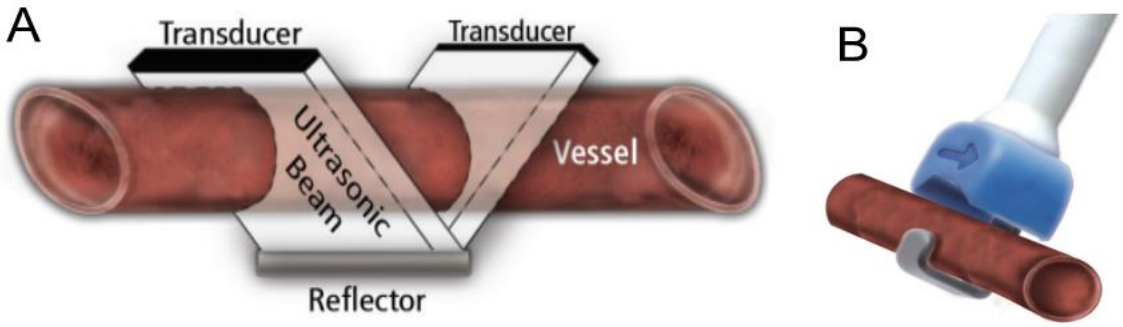

Figure 2.6: Time transit ultrasound flow probe. The two transducer sensors pass the ultrasonic beam back and forth (A) intersecting the blood flowing through the vessel. Flow probe wrapped around a vessel (B), measures the "transit time" required for the ultrasonic beam to pass from one transducer to the other, giving us the difference in "transit time" as a measure of cardiac output. Image adapted from Transonic PV workbook SP-1-wb Rev A 2019.

Lastly, both the catheters and flow probe are soaked into tergazyme for ≥ 30 min immediately after each surgery and cleaned with fresh deionized (DI) water for ≥ 2 minutes.

2.5. Constitutive Model of the Arterial Systems

To understand the physiology of the arterial system, we used a two and three element Windkessel model also known as lumped model in our study. Section 2.5.1 goes more in depth about the Windkessel model used in this study. Section 2.5.2 describes the numerical implementation of the two and three element Windkessel model and shows how the resistance and compliance parameters changes in the pulmonary vasculature as PAH progress overtime.

2.5.1. Modeling Approach: Two Element Windkessel Model

To understand the changes in pulmonary vasculature properties during the early and later stages of PAH, we used a two and three-element Windkessel model. These lumped models are derived from an electrical circuit analogy where each element in the circuit has a physiological relevance to the arterial property. For example, resistance in the electrical circuit represents the arterial and peripheral resistance properties of the vessel. The capacitance element in the circuit represents volume compliance of the vessels that can store blood volume during systole [35]. The resistance offered by the pulmonary circulation is known as the pulmonary vasculature resistance and the systemic circulation resistance is known as systemic vascular or total peripheral resistance. In this section, we will derive the mathematical equations for the two and three element Windkessel model using Kirchhoff's current law.

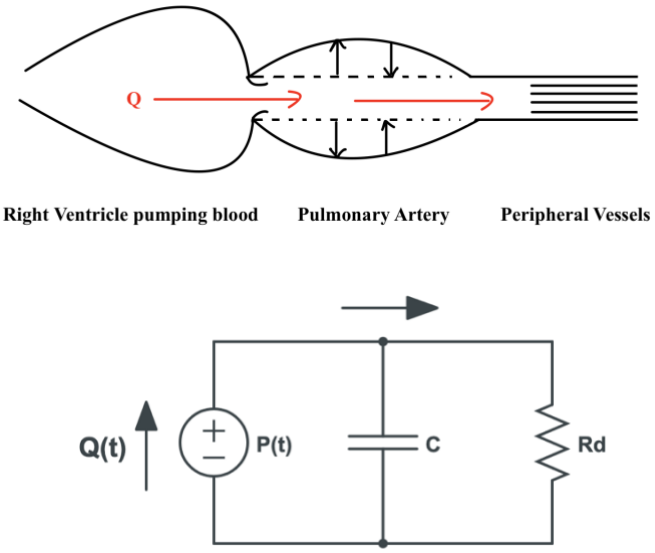

Figure 2.7: (Top) Schematic representation of the ventricular ejection of blood into the pulmonary arterial system. (Bottom) An electrical analogy of a two-element Windkessel model with two parameters: Compliance (C), and distal Resistance(R_d).

The two-element Windkessel model consists of two elements - a resistance (mmHg*min/ml) and compliance (ml/mmHg) - that describes the physiological properties of an arterial system. During systole, the flow of blood from the right ventricle to the pulmonary vasculature is analogous to the current flowing through the electrical circuit. The change in voltage is analogous to the change in pressure at the proximal and distal end of a pulmonary vessel. The resistance refers to the measure of force that counteracts the flow of blood in a vessel, similar to the flow of current in a circuit.

Therefore, the governing equation for both the two and three element Windkessel model can be derived using the Kirchhoff's current law:

For two-element Windkessel model, the Kirchhoff's current law can be written as:

$$Q(t) = Q_1(t) + Q_2(t) \tag{2.2}$$

where, $Q(t)$ is the flow of blood out of the heart and $Q_i(t)$ is the flow into each branch of the Windkessel model.

We know,

$$Q_1(t) = C \frac{dP(t)}{dt} \tag{2.3a}$$

$$Q_2(t) = \frac{P(t)}{R_d} \tag{2.3b}$$

where C is the compliance, P is the pressure and R_d is the distal resistance.

Substituting Equation 2.3a and 2.3b into Equation 2.2 and diving both side by $\frac{1}{c}$ we get,

$$\frac{Q(t)}{C} = \frac{dP(t)}{dt} + \frac{P(t)}{R_d C} \tag{2.3c}$$

Equation 2.3c can also be rearranged as:

$$\frac{dP(t)}{dt} = \frac{Q(t)}{c} - \frac{P(t)}{R_d C} \tag{2.4}$$

2.5.2 Modeling Approach: Three-element Windkessel model

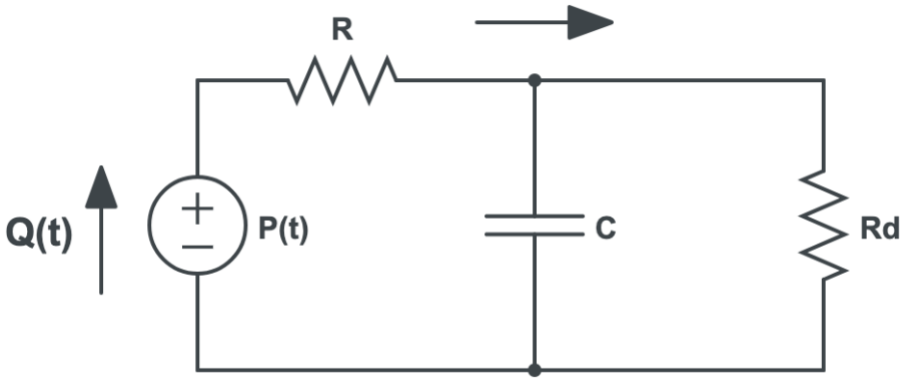

Figure 2.8: An electrical analogy of a three-element Windkessel model with three parameters: Proximal resistance (R), Compliance (C), and distal Resistance (R_d).

Unlike two-element, a three-element Windkessel model consists of proximal resistance (R) parameter added in series to the compliance (C). In the two element Windkessel model, the compliance and distal resistance parameter is used to describe the physiological properties of the vasculature as described in Section 2.5.1. However, in the three element Windkessel model, proximal resistance accounts for the pulsatile flow of the blood as it gets ejected out from the right ventricle into the pulmonary arteries. The combination of proximal resistance with the compliance property of a vasculature can be used to describe the pulsatile flow of the blood in the large vessels [9]. This pulsatile flow in the large pulmonary vessels needs to be converted into a steadier flow further down to the distal vessels which is represented by parameter (R_d) in the three-element Windkessel model. The number of electrical elements added to the model leads to either two or three element Windkessel model. Moreover, a four-element Windkessel model has also been proposed in literatures with an additional element known as inductance, added to the three-element

Windkessel model [9], [21]. The inductance is used to describe the inertial aspect of the pulmonary system which is not our area of focus.

The governing equation for the three-element Windkessel model can also be derived using Kirchhoff's current law as shown in Section 2.5.1.

$$\frac{dP(t)}{dt} + \frac{1}{R_d C} P(t) = \left(\frac{1}{C} + \frac{R}{R_d C}\right) Q(t) + R\frac{dQ(t)}{dt} \tag{2.5}$$

Thus, an analytical solution for the generalized two, three or four element Windkessel model can be found within the same form as shown in Equation 2.6

$$P(t) = P_0\, e^{\frac{t}{R_d C}} + e^{\frac{t}{R_d C}} \int_0^t e^{\frac{\tau}{R_d C}} q(\tau) d\tau \tag{2.6}$$

2.6. Numerical Methods

In this section, we will summarize different types of numerical approaches used to analyze the *in vivo* hemodynamic data in MATLAB. Section 2.6.1 will go more into depth about the Fourier series analysis of the flow data using Moore-Penrose pseudo inverse method. Section 2.6.2 will emphasize on the explicit fourth order Runge-Kutta method. Section 2.6.3 will discuss important built in MATLAB algorithms used in our three-element Windkessel model for parameter estimations and error.

2.6.1. Analysis of Input Flow Signal Using Fourier Series

The hemodynamic measurements - pressure and flow were acquired using techniques and procedures described in section 2.2, 2.3 and 2.4. Both flow and pressure were measured over many cardiac cycles and a cycle with the least inference from the respiratory cycle and noise was chosen for the analysis. The governing equations for both two and three-element Windkessel models (Equation 2.4 & 2.5) were derived from Kirchhoff's conservation law.

The driving term in both the two and three-element Windkessel model is governed by flow. The Fourier series was therefore used as a means to represent this periodic signal of a flow wave into an infinite sum of a sine and a cosine wave. The primary reason for using a Fourier series is that it helps us better analyze the signal and predict the outcome more accurately than the original domain signal. The Fourier series of the form shown below was used in both of our models to allow for the continuous time sampling of the data

$$Q(t) = c + \sum_{k=1}^{N} a_k \sin(k\omega_0 t) + b_k \cos(k\omega_0 t) \tag{2.7}$$

where, ω_0 is a frequency signal calculated using $\omega_0 = \frac{\pi}{T}$, T is a period of cardiac cycle.

Using Fourier series in Equation 2.7 allows us to analytically differentiate the input data without using any numerical application. For instance, the first derivative of the Fourier form using Equation 2.7 is:

$$\frac{dQ(t)}{dt} = \sum_{k=1}^{N} a_k \, k \, \omega_0 \cos(k\omega_0 t) - b_k \, k \, \omega_0 \sin(k\omega_0 t) \tag{2.8}$$

Using MATLAB, a *func* with a Fourier series of form Equation 2.7 was made, and the order of Fourier series was iteratively increased until the error between the original domain flow signal and the approximation domain flow signal was less than 0.001. The goal was to find the parameters of Fourier series such that the approximated data is as close as possible to the true flow data. Therefore, during each iteration, the unknown parameters a_k , b_k and c was determined using Moore-Penrose pseudoinverse method. Using Moore-Penrose pseudo-inverse method to solve the system, the Fourier function was written in state-space form:

$$\begin{bmatrix} \sin(\omega_0 t_1) & \cos(\omega_0 t_1) & \sin(2\omega_0 t_1) & \dots & \cos(k\,\omega_0 t_1) & 1 \\ \vdots & \vdots & \vdots & \dots & \vdots & \vdots \\ \sin(\omega_0 t_m) & \cos(\omega_0 t_m) & \sin(2\omega_0 t_m) & \dots & \cos(k\,\omega_0 t_m) & 1 \end{bmatrix} \begin{bmatrix} a_1 \\ b_1 \\ a_2 \\ \vdots \\ b_k \\ c \end{bmatrix} = \begin{bmatrix} Q(t_1) \\ \vdots \\ Q(t_m) \end{bmatrix} \quad (2.9)$$

Here,

A is a matrix that contains all the sinusoidal terms with dimensions $A \in (m \times k+1)$

$\overline{x}$ is a vector with parameters $\overline{x} \in \begin{Bmatrix} a_k \\ b_k \\ c \end{Bmatrix}$

$\overline{b}$ is also allocated to be a vector with data at any time point t_m

This gives the non-square matrix equation,

$$A\,\overline{x} = \overline{b} \quad (2.10a)$$

which can be made a square matrix using Moore- Penrose pseudoinverse method shown below:

$$(A^T A\overline{x})^{-1} \times (A^T A)\overline{x} = (A^T A)^{-1} \times A^T\,\overline{b} \quad (2.10b)$$

where, $(A^T A\overline{x})^{-1} \times (A^T A)$ is an identity matrix (I) giving us,

$$\overline{x} = (A^T A)^{-1} \times A^T \overline{b} \tag{2.11}$$

Therefore, the Moore-Penrose pseudo-inverse method can be used to convert the non-square matrix into a square matrix. The mean square error (MSE) was then calculated between the original and approximated flow data points using the equation below:

$$MSE = \frac{1}{n} \sum_{i=1}^{n} (y_i - \tilde{y}_i)^2 \tag{2.12}$$

where y_i is the measured flow and $\tilde{y}_i$ is the approximated flow data points from Fourier series.

2.6.2. Numerical Model Solving Using Runge-Kutta Method

In order to solve the nonlinear system of ordinary differential equation analytically, we use explicit or implicit Runge-Kutta (RK) method. Both two and three-element Windkessel models were solved using an explicit fourth order Runge-Kutta method using an *ode45* function in MATLAB. This built-in algorithm in MATLAB, adapts the time step by estimating the fifth order error also known as truncation error $\theta\ (h^5)$ and total accumulation error $\theta\ (h^4)$. The explicit fourth order RK method for a model defined by $\frac{dP(t)}{dt} = F(t, \bar{P};\ \theta)$ is shown below:

$$P_{k+1} = P_k + \frac{1}{6} (K_1 + 2K_2 + 2K_3 + K_4) + \theta(h^5) \tag{2.13}$$

where

$$K_1 = hF(t_k, P_k) \tag{2.14}$$

$$K_2 = hF\left(t_k + \frac{h}{2}, P_k + \frac{K_1}{2}\right) \tag{2.15}$$

$$K_3 = hF\left(t_k + \frac{h}{2}, P_k + \frac{K_2}{2}\right) \tag{2.16}$$

$$K_4 = hF(t_k + h, P_k + K_3) \tag{2.17}$$

Here, K_1 is the increment based on the slope at the beginning of the interval using P_k . K_2 is at the increment at midpoint using $P_k + \frac{K_1}{2}$. K_3 is also at the midpoint but using $P_k + \frac{K_2}{2}$. Lastly, K_4 is the increment at the end of the interval using $P_k + K_3$. The time interval from $[a, b]$ is partitioned into *N* equally spaced division with a length of *h*, the time steps defined as $h = \frac{(b-a)}{N}$.

This formula predicts the value of P_{k+1} using the current P_k plus the weighted average of four increments with the fifth order truncation error. The primary reason for choosing the *ode45* function to approximate a solution is because our first order differential equations is not stiff. The algorithm that is commonly used in MATLAB to solve the stiff ordinary differential equations is *ode15*.

2.6.3. Parameter Estimations Using Built- in MATLAB Algorithms

We solved for the nonlinear first order differential equation in MATLAB using an *ode45* algorithm. *ode45* is an adaptive time step function so the solved time points and the true pressure data points do not align. To account for this issue, the solved solution is linearly interpolated between the adjacent time points using *interp1*. The *interp1* command interpolates the data between the data points so we can find values at the intermediate points of a first order function that underlies the data.

The mean square error between the data and the interpolated model was calculated and the parameters were updated to best fit our data using a built in *fminsearch* function in MATLAB. *fminsearch* function takes in the scalar function of multiple parameters with their initial guesses as an input and gives us optimized parameters as an output. For the three-element Windkessel model, the initial guesses for R_d and C was done using the optimized values from the two-element model. R was estimated from experimenting with the model itself. This iterative process of updating a parameter was restarted until the mean squared difference between the initial and optimized model parameter was less 0.0001 ensuring stability and accuracy of the model. Lastly, the root mean square percent error (RMSPE) between the measured data points and the model data points was calculated using:

$$RMSPE(\%) = 100 * \sqrt{\frac{1}{n} \sum \left(\frac{y_i - \hat{y}}{y_i}\right)^2} \tag{2.18}$$

where y_i is the measured pressure data and $\hat{y}$ is the estimated pressure from a three element Windkessel model.

2.7. Sensitivity Analysis for Each Windkessel Parameters

Sensitivity Analysis is used to understand the impact of parameters on the model output. The sensitivity equations for our model were analytically derived and numerically solved. The sensitivity equations were derived as follows:

Given the model's form $\frac{dP(t)}{dt} = F(t, \bar{P};\ \theta)$, the sensitivity equations for a given parameter i are $\emptyset_i = \frac{\partial P}{\partial \theta_i}$. Now, in order to derive the sensitivity equations for the model, the local Jacobian matrix with respect to each parameter θ was computed:

$$\frac{d\emptyset_i}{dt} = \frac{d}{dt}\frac{\partial P}{\partial \theta_i} \tag{2.19}$$

Which can be expanded using chain rule:

$$\frac{d\emptyset_i}{dt} = \frac{d}{dt}\frac{\partial P}{\partial \theta_i} = \frac{\partial F}{\partial P}\frac{\partial P}{\partial \theta_i} + \frac{\partial F}{\partial \theta_i} \tag{2.20}$$

The sensitivity matrix for two and three element Windkessel model in state-space form can therefore be written as:

For two element model:

$$\begin{bmatrix}\emptyset_1 \\ \emptyset_2\end{bmatrix} = \begin{bmatrix}\frac{\partial P}{\partial R_d} \\ \frac{\partial P}{\partial C}\end{bmatrix} \quad \begin{bmatrix}\frac{d\emptyset_1}{dt} \\ \frac{d\emptyset_2}{dt}\end{bmatrix} = \begin{bmatrix}-\frac{1}{R_d\,C} & 0 \\ 0 & -\frac{1}{R_d\,C}\end{bmatrix}\begin{bmatrix}\emptyset_1 \\ \emptyset_2\end{bmatrix} + \begin{bmatrix}\frac{P(t)}{R_d^2 C} \\ \frac{P(t)}{R_d C^2} - \frac{Q(t)}{C^2}\end{bmatrix} \tag{2.21}$$

For three- element model:

$$\begin{bmatrix} \emptyset_1 \\ \emptyset_2 \\ \emptyset_3 \end{bmatrix} = \begin{bmatrix} \frac{\partial P}{\partial R_d} \\ \frac{\partial P}{\partial C} \\ \frac{\partial P}{\partial R} \end{bmatrix} \quad \begin{bmatrix} \frac{d\emptyset_1}{dt} \\ \frac{d\emptyset_2}{dt} \\ \frac{d\emptyset_3}{dt} \end{bmatrix} = \begin{bmatrix} -\frac{1}{R_d\, C} & 0 & 0 \\ 0 & -\frac{1}{R_d\, C} & 0 \\ 0 & 0 & -\frac{1}{R_d\, C} \end{bmatrix} \begin{bmatrix} \emptyset_1 \\ \emptyset_2 \\ \emptyset_3 \end{bmatrix} + \begin{bmatrix} \frac{P(t)}{R_d^2 C} - \frac{RQ(t)}{R_d^2 C} \\ \frac{P(t)}{R_d C^2} - \frac{Q(t)}{C^2}\left(\frac{R}{R_d} + 1\right) \\ \frac{Q(t)}{R_d\, C} + \frac{dQ}{dt} \end{bmatrix} \quad (2.22)$$

To compare the sensitivity of individual parameters to the model output, sensitivity analysis was performed using matrix Equation 2.21 and 2.22. Additionally, a relative sensitivity was obtained by normalizing the sensitivity matrix by both the model output and each corresponding parameter,

$$F(t, \bar{P};\ \theta) = \frac{\theta_i}{P(t;\ \theta_i)}\ \frac{dP(t;\ \theta)}{d\theta_i} for\ A\ \neq 0\ and\ \theta_i\ \neq 0 \quad (2.23)$$

Here $F(t, \bar{P};\ \theta)$ is a differentiable function.

The structural identity of the model parameters $\emptyset_i$ were analyzed by determining the rank of the sensitivity matrix. The function *rank* in MATLAB provides an estimate of the number of linearly independent rows and columns of the matrix. If the *rank* of the phi ($\emptyset$) parameter for a 2-element Windkessel model is 2 then it is structurally identifiable which means that the rows and columns of this matrix are linearly independent for all time (t). They are also invertible. Similarly, if the *rank* of 3-element Windkessel models is 3, then it is structurally identifiable. Moreover, if they are linearly independent, they must be structurally identifiable. Lastly, to numerically rank how sensitive the model output $P(t;\ \theta_i)$ is to perturbations in the parameter, the *2-norm* function in MATLAB is used which can be calculated as,

$$\left\| \frac{dP(t;\theta)}{d\theta_i} \right\|_2 \text{ where, } \theta_i = \{ R, R_d, C \} \tag{2.24}$$

Conducting sensitivity analysis of the optimized parameters allows us to understand the contribution of each parameter in the model output at the parameter space that most closely represents the actual experimental data. The most sensitive parameter will give the largest value in magnitude and the least sensitive parameter will be the one with smaller magnitude. Although any parameters can be sensitive to the model, it shouldn't be assumed that they could also be structurally identifiable. In those cases, correlation could exist among the parameters which can be further studied by computing the correlation matrix.

2.8. Statistical Analysis

In mathematical modeling we often try to build a physical model to study the physiological system as accurately as possible. This sometimes may result in a large number of parameters with uncertainties. Statistical analysis can therefore be used to quantify the uncertainty of estimated model parameters. Thus, to assess the estimated model parameters, standard errors, and confidence intervals for each parameter a statistical model can be used:

$$A_j = F_j(\overline{\theta}) + \epsilon_j \tag{2.25}$$

where A_j is the model output of the optimized parameter, $F_j(\overline{\theta})$ is the model output at the initial parameters and ϵ_j the measurement error. ϵ_j are assumed to be independent and identically distributed (i.i.d.) random variables with mean $\mathrm{E}[\epsilon_j] = 0$ and constant variance $var[\epsilon_j] = {\sigma_0}^2$

where $\sigma_0{}^2$ is unknown. For the continuously differentiable data, the standard nonlinear approximation theory for asymptotic distribution can be applied. This theory states that the sampling distribution $\hat{\theta}(a)$ for the estimate $\hat{\theta}$ follows an n-dimensional multivariable Gaussian distribution with $\mathrm{E}[\hat{\theta}\,] = \theta_0$. Hence, due to the large number of data points used in the model, it is assumed that the optimized parameters well approximate the distribution mean and the covariance of the distribution using the sensitivity matrix shown in Equation 2.21 and 2.22. The sampling distribution therefore is modeled using

$$\hat{\theta}_n = \mathcal{N}_n(\theta_0, \Sigma_0) \tag{2.26}$$

where n is the number of parameters, θ_0 is the distribution mean and Σ_0 is the co-variance which can be calculated as:

$$\Sigma_0 = \sigma_0{}^2 \left(\chi\ (\theta_0)^T \chi(\theta_0)\right)^{-1} \tag{2.27}$$

and

$$\sigma_0{}^2 = \frac{1}{n-n_p} \sum_{j=1}^{n} \left| A(t_j;\ \theta) - a_j \right|^2 \tag{2.28}$$

Here, n_p is the number of model parameters, $\chi\ (\theta_0)$ is the $n \times np$ sensitivity matrix, and $\sigma_0{}^2$ is the standard deviation.

Finally, the confidence interval for each parameter can be computed using standard error and covariance matrix Equation 2.27.

$$SE_k(\theta_0) = \sqrt{\Sigma_{kk}(\theta_0)} \tag{2.29}$$

where the standard error of each estimated parameter theta is the square root of the diagonal entries of the covariance matrix Σ_0. Thus, the confidence interval for the k^{th} parameter, at a level of 95% confidence interval was formulated using:

$$\left[\theta_k - t_{1-\frac{\alpha}{2}} SE_k(\theta_0) \ , \ \theta_k + t_{1-\frac{\alpha}{2}} SE_k(\theta_0)\right] \tag{2.30}$$

where, $t_{1-\frac{\alpha}{2}}$ is the critical value computed from the student's t distribution with $n - n_p$ degrees of freedom. For the large set of datasets, degrees of freedom $\sim \infty$. Hence $t_{1-\frac{\alpha}{2}} \approx 1.96$.

Two - way ANOVA Analysis using JMP pro Software

In order to compare the means of the model parameters and how they depended on sex and treatment, we performed a two-way ANOVA in JMP Pro statistical software (version 14, SAS Institute Inc., NC). A two-way ANOVA is a statistical test used to determine the effect of multiple independent categorical variables on a continuous variable. It compares the mean differences between variables and uses this information to check the variances in addition to the degree of interaction between two independent variables (sex, treatment group) on the dependent variable (compliance, proximal and distal resistances). The main assumptions underlying the two-way ANOVA test is that the two variables for testing should be independent of each other and have a normal distribution. Therefore, in order to test for the differences in sex and treatment groups, a

two-way ANOVA was used followed by the Dunnett's post hoc test in JMP software. The Null hypothesis for our study is as follows:

Null hypothesis #1: there are no difference in the compliance, proximal and distal resistance mean due to sex.

Null hypothesis #2: there are no differences in the compliance, proximal and distal resistance mean due to SuHx treatment.

Null hypothesis #3: there is no interaction effects between the sex and treatment group. The formulation used to calculate the two-way ANOVA is as follows:

$$\text{Sum of Squares (SS)} = \sum(x - \bar{x})^2 \tag{2.31}$$

$$\text{Mean Square Difference (MSD)} = \frac{\sum(x-\bar{x})^2}{df} \tag{2.32}$$

where x is the measurement, $\bar{x}$ is the group mean and df is the degrees of freedom.

For non-normally distributed data, nonparametric statistical tests such as Wilcoxon-Kruskal Wallis statistical test are used followed by the Dunnett's post hoc test. Statistical significance for our study was determined at a level of $\alpha = 0.05$. Graphs were then generated using GraphPad Prism software (version 8.4.3, GraphPad Software, CA).

3. Results

SuHx treated male, female and ovariectomized female rats were used in our research to study PAH. *In vivo* hemodynamic measurements were acquired using PV and dual pressure catheters shown in Section 2.2 and Section 2.3 and analyzed using a two and three-element Windkessel model as described in Section 2.5.1 and 2.5.2. This section presents the results generated by using the constitutive three-element Windkessel model.

3.1. Input Flow Data Fitting Using Fourier Series

The governing equation of the three element Windkessel model takes in flow and the first derivative of flow as an input. The flow data acquired from the *in vivo* hemodynamic studies from each individual rats were grouped together based on their specific sex and treatment group. In order to allow for the continuous time sampling of the data, the flow was fitted to the Fourier series within a mean square error of 0.001. Additionally, the average flow and pressure for each sex and treatment groups of rats were also calculated. Figure 3.1, 3.2 and 3.3 shows the plot of average flow fitted to the Fourier series and its analytical first order derivative for normotensive (control) and hypertensive rats (week-8 PAH).

Male

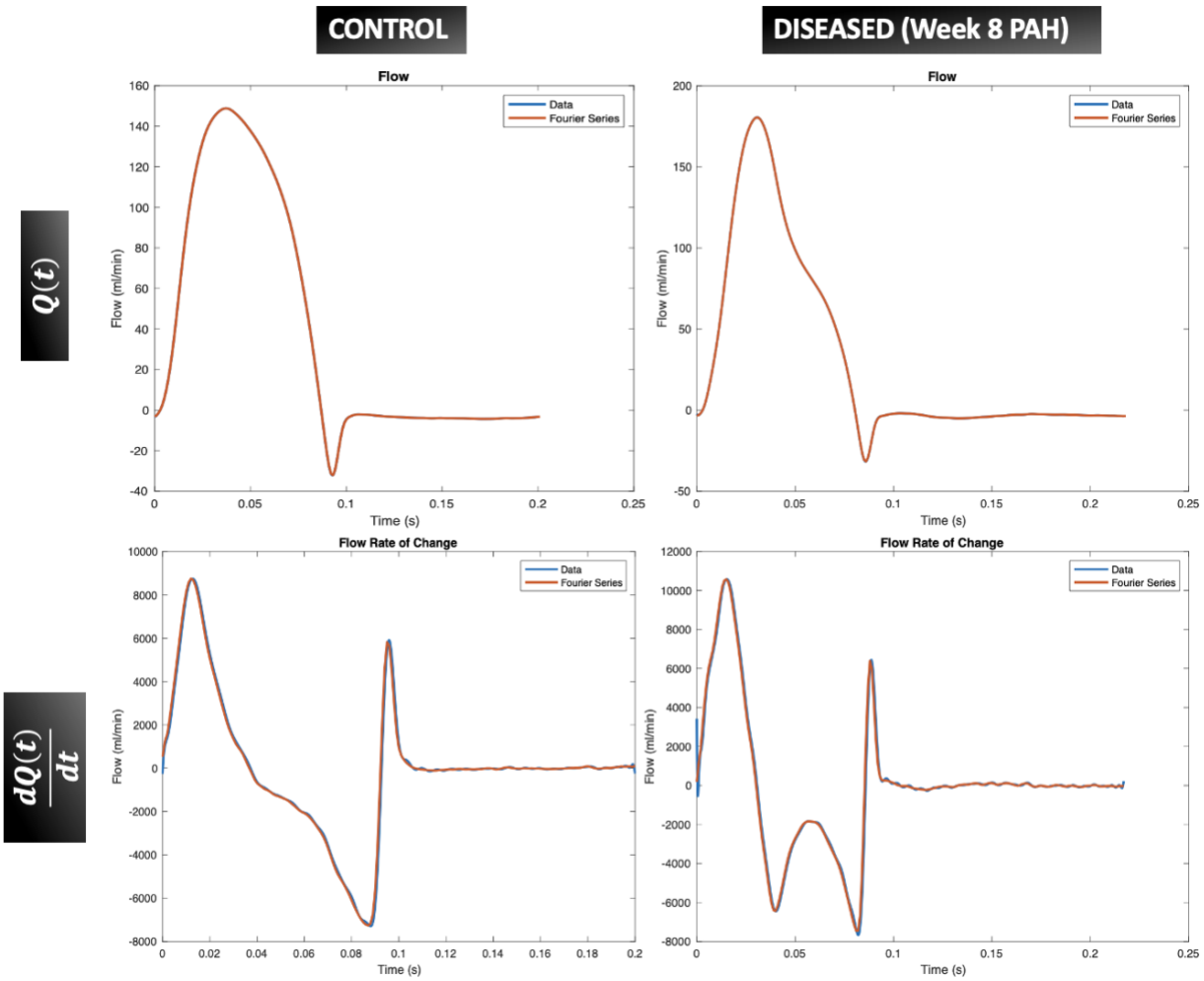

Figure 3.1: Fourier Fit of the flow data. For both the control and diseased male rats, the Fourier series fits of flow data and the rate of change of flow are plotted with flow data and its respective numerical derivatives with the mean square error threshold of < 0.001.

Female

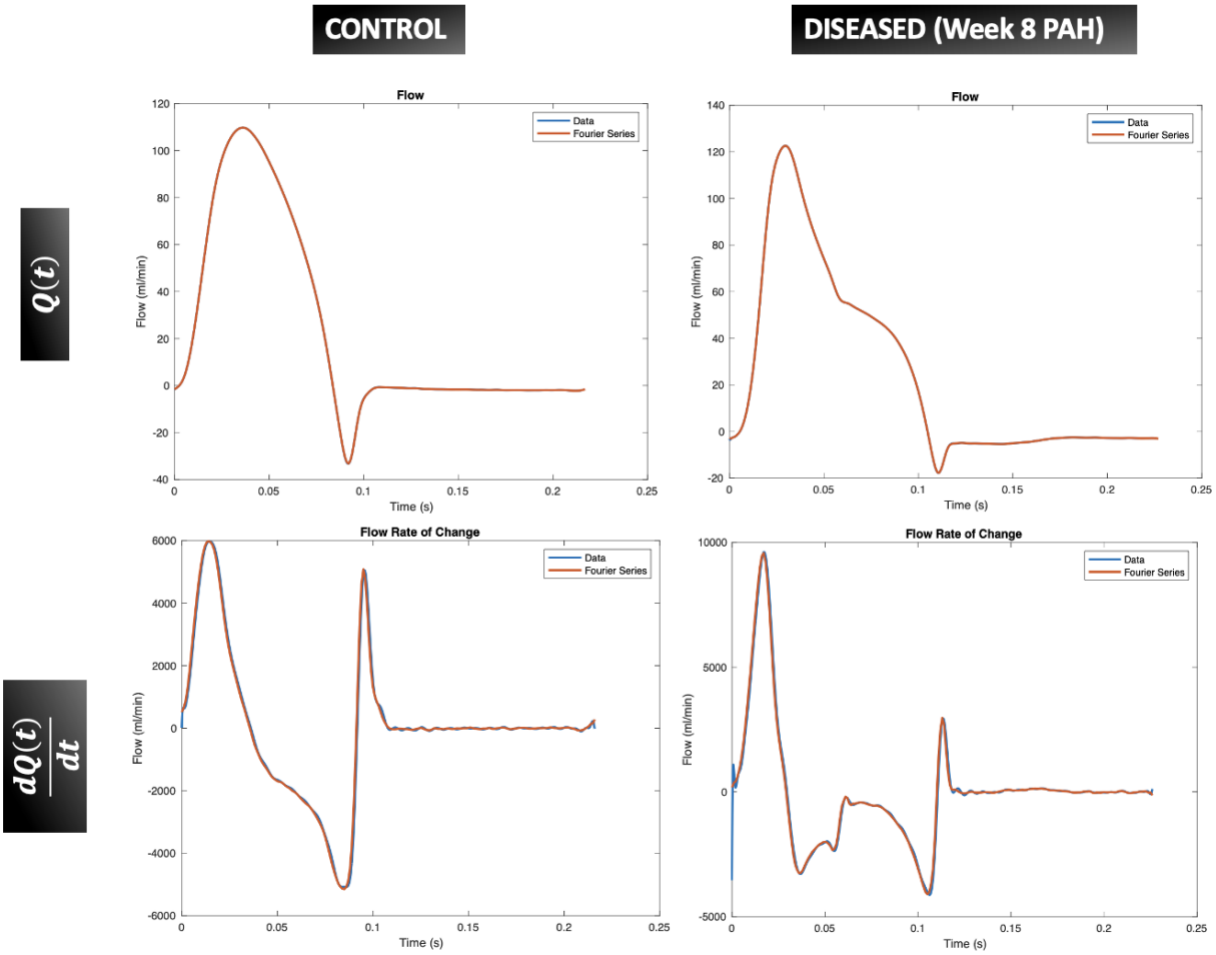

Figure 3.2: Fourier Fit of the flow data. For both the control and diseased male rats, the Fourier series fits of flow data and the rate of change of flow are plotted with flow data and its respective numerical derivatives with the mean square error threshold of < 0.001.

OVX Female

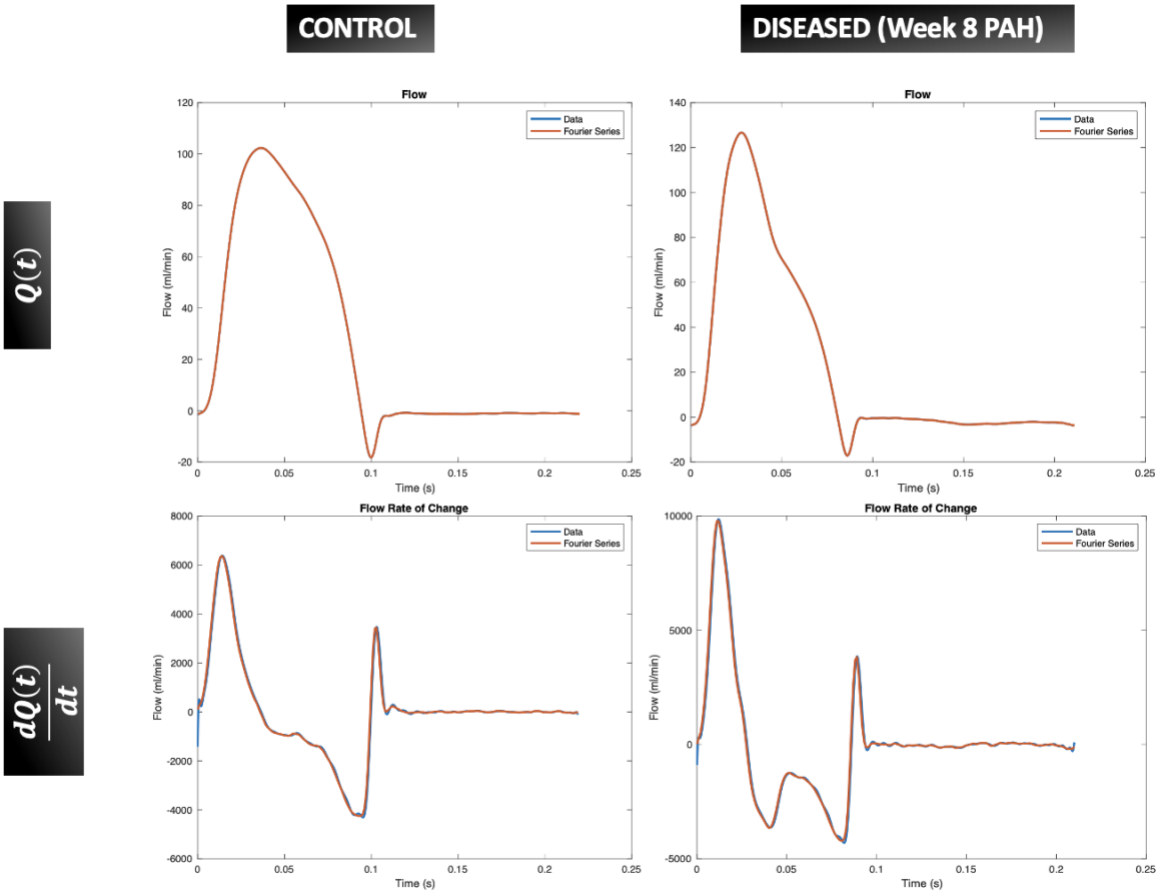

Figure 3.3: Fourier Fit of the flow data. For both the control and diseased male rats, the Fourier series fits of flow data and the rate of change of flow are plotted with flow data and its respective numerical derivatives with the mean square error threshold of < 0.001.

3.2. Model Fitting and Parameter Estimation

After the Fourier analysis of the flow data and its first derivative, the three element Windkessel model was used to individually fit pressure data acquired from the *in vivo* hemodynamic studies. The R, R_d and C parameters estimated by the three-element Windkessel model. Additionally, the three-element Windkessel model again was used to fit the average pressure data for each sex and treatment groups. The parameters estimated by the model fitted to the average pressure data were compared to the average R, R_d and C values of the individually fitted pressure data. Because the average values of R, R_d and C were about the same, the average pressure data was used for further analysis. Moreover, week 4 and week 8 were chosen because the difference in their mPAP is statistically insignificant ($p < 0.01$) for different groups of rats (Figure 3.4).

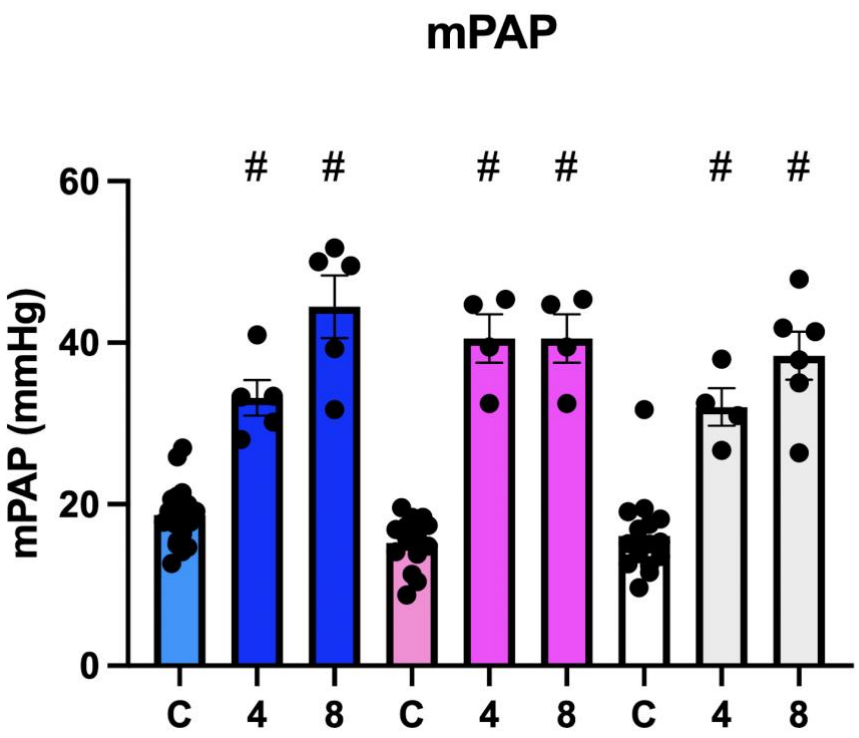

Figure 3.4: The changes in mPAP of male (blue), female (pink) and OVX female (white) rats at different stages of PAH (week 4 and week 8). Data shown as mean ± SE, # $P < 0.01$ compared with their respective control group. SuHx- sugen-hypoxia. C- control.

The pressure waveform estimated by the three-element Windkessel model is presented in Figure 3.5. The optimized Windkessel parameters are shown in Table 2. In order to compare the precision of the pressure waveform predicted by this model for different treatment groups and sexes, the root mean square percent error (RMSPE) was also calculated as shown in Table 1.

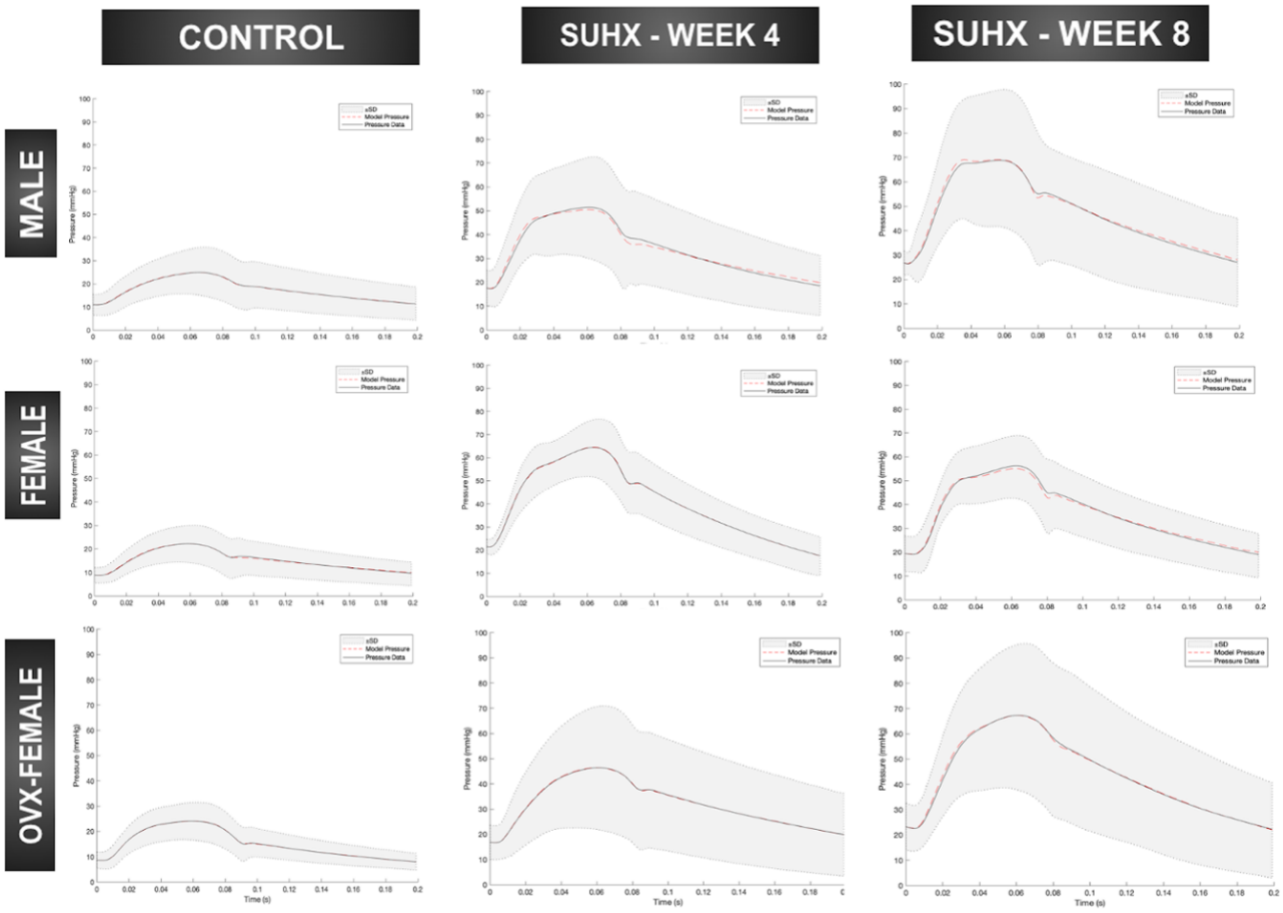

Figure 3.5: Pressure waveform estimated using a three-element Windkessel model fitting the measured pressure data spanning 95% confidence interval within two standard deviations. Errors in the model fits were quantified via RMSPE presented in table 1.

Table 1: Root mean square percent error (RMPSE) calculated for the three-element Windkessel model for different groups of rats at different stages of PAH

	Treatment Groups **RMSPE**		
Sexes	**Control**	**Week - 4**	**Week - 8**
Male	0.458%	3.75%	2.198%
Female	1.424%	0.238%	2.340%
OVX-Female	0.391%	0.365%	0.372%

Table 2: Summary of optimized Windkessel parameters estimated by a three-element Windkessel model for each individual sexes - male, female, OVX and treatment groups- Control, Week-4, Week-8 - spanning 95% confidence interval within two standard deviations.

	Groups								
	Control (N = 11)			Week-4 (N = 5)			Week-8 (N = 5)		
	R (mmHg min/mL)	R_d (mmHg min/mL)	C (mL/mmHg)	R (mmHg min/mL)	R_d (mmHg min/mL)	C (mL/mmHg)	R (mmHg min/mL)	R_d (mmHg min/mL)	C (mL/mmHg)
Male	0.041 ± 0.001	0.432 ± 0.005	0.504 ± 0.016	0.158 ± 0.008	1.751 ± 0.021	0.117 ± 0.004	0.129 ± 0.008	1.438 ± 0.025	0.138 ± 0.005
Female	0.052 ± 0.001	0.695 ± 0.007	0.339 ± 0.009	0.105 ± 0.010	1.142 ± 0.024	0.109 ± 0.006	0.152 ± 0.023	1.546 ± 0.054	0.112 ± 0.009
OVX-Female	0.093 ± 0.002	0.481 ± 0.008	0.346 ± 0.014	0.109 ± 0.005	1.581 ± 0.021	0.131 ± 0.004	0.102 ± 0.008	2.201 ± 0.023	0.071 ± 0.004

Similarly, the parameters estimated by the three element Windkessel model exhibited statistically significant differences between sexes and treatment groups and reflected the relevant physiological changes as disease progresses.

Proximal resistance (R) was not statistically significant different ($p > 0.05$) due to sex. There was a significant difference in the control and treatment groups (SuHx week 4 and week 8) ($p < 0.05$) in male rats. Similarly, the distal resistance (R_d) was not statistically significantly different between sexes. However, the difference between the control and treatment group for SuHx week 4 or week 8 was noted ($p < 0.05$) in males and ovariectomized rats. Although the resistance was not statistically different in sex, difference between the control and treated group showed that they do change. In other words, the resistance increases significantly as the PAH progresses over time. Figure 3.6A and 3.6B shows a significant increase of proximal and distal resistance at week 4 and then a slight decrease only in males at week 8. For all the other sexes, the increase in both the proximal and distal resistances were statistically insignificant.

Compliance (C) was statistically significantly different between male and female rats ($p = 0.0237$) and between OVX female and male rats ($p = 0.0186$). Significant difference between control and treatment group week 4 and week 8 in males and females ($p < 0.05$). As shown in Figure 3.6C, compliance seems to decrease sharply by as early as week 4 and stays about the same as PAH progresses in all groups. As both the resistances slowly tend to increase first in males, the compliance seems to sense PAH earlier, hence sharply decreases in all three sexes. Week 4 and week 8 were not significant for any of the three-element Windkessel model.

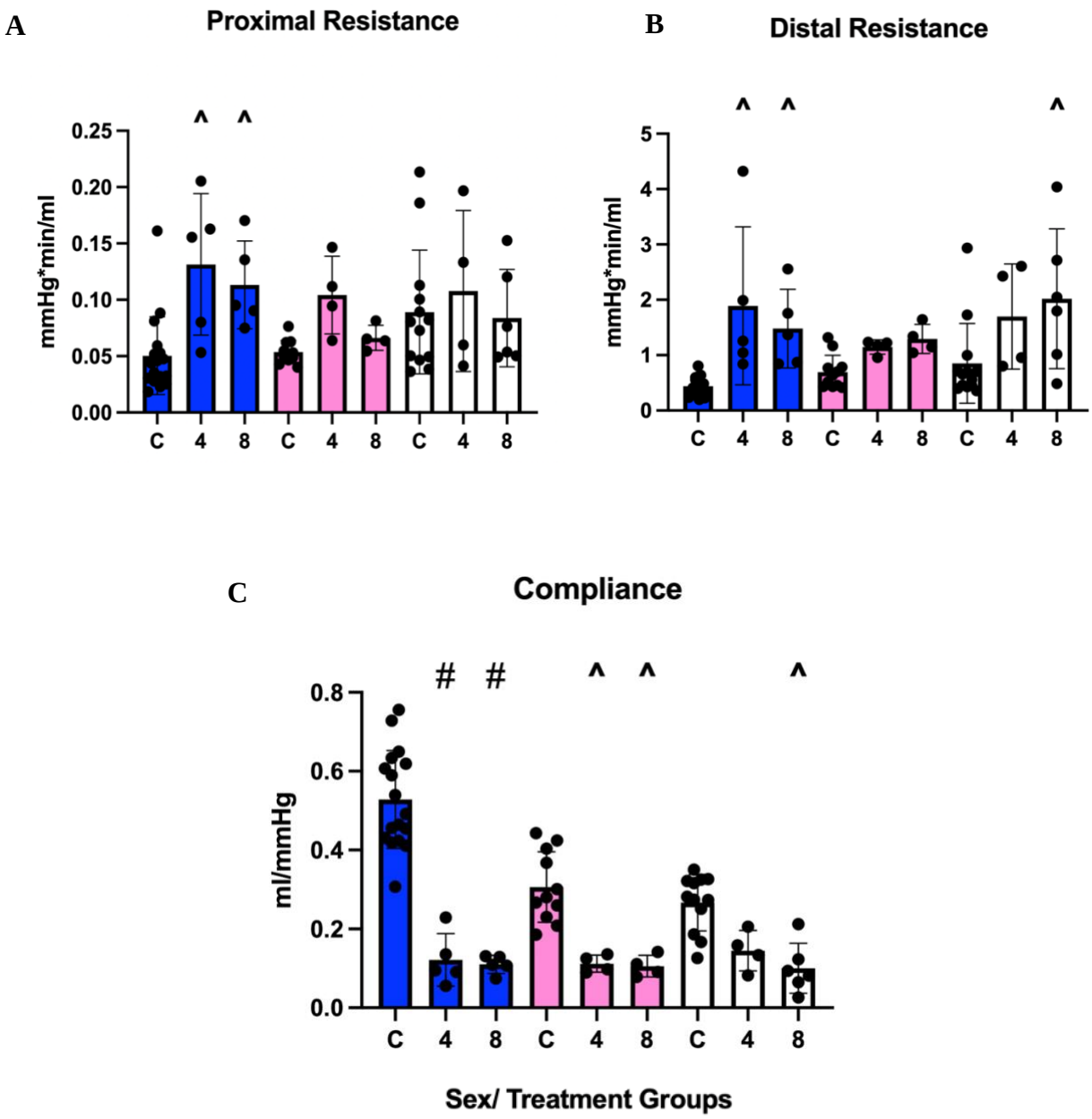

Figure 3.6: R, R_d and C parameters estimated using a three-element Windkessel model of at weeks 4 and 8 of SuHx in male (blue), female (pink), and OVX female (white) rats. (A) A significant increase in proximal resistance by week 4 is observed only in males. (B) There is a significant increase in the distal resistance from control to week 4 or week 8 in male and ovariectomized female rats. (C) There is a significant compliance decrease in male and female rats due to PAH induction. The compliance decreases significantly by as early as week 4 and plateaus as PAH progresses in all three groups of rats. Data shown as mean $\pm$ SE, ^p <0.05 and # p < 0.01 compared with the control group. SuHx- sugen-hypoxia.

3.3. Sensitivity Plots of The Model Parameters

Figure 3.7 shows the relative sensitivity analysis that were performed for each sex and treatment groups. Because week 4 and week 8 groups were not statistically different, we only focused on control and week 8. The R, R_d and C parameters had their own respective sensitivity response to the model output. For both the control and diseased group (SuHx week 8 PAH) regardless of the sex differences and diseased state, R_d held the greatest influence over the model output. This was followed by the compliance parameter C and R. Table 3 shows the relative sensitivities 2-norms for different groups of rats as PAH progresses overtime. Each parameter is ranked based on their respective sensitivities.

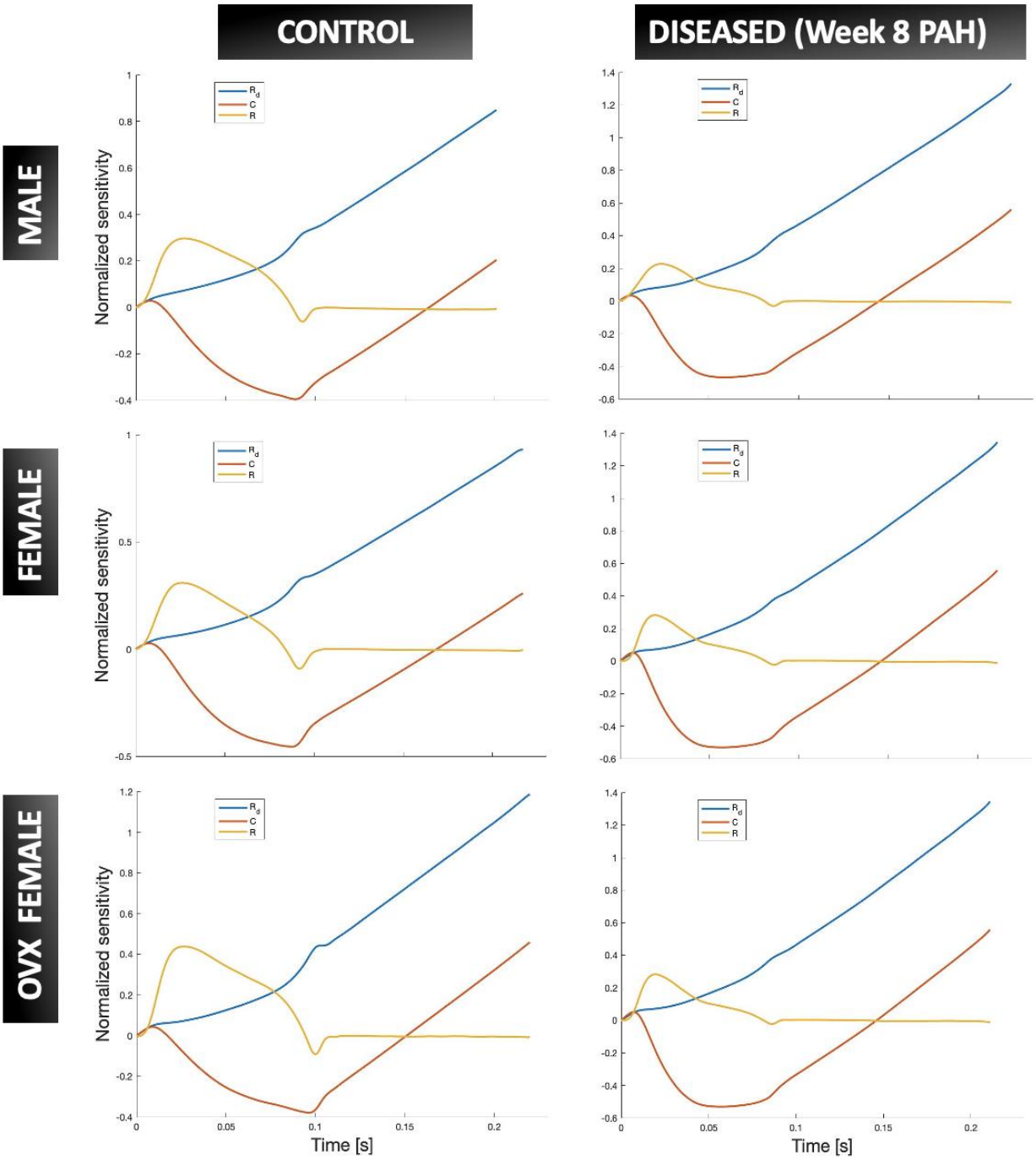
CONTROL
DISEASED (Week 8 PAH)
MALE
FEMALE
OVX FEMALE
Normalized sensitivity
Time [s]
R_d
C
R

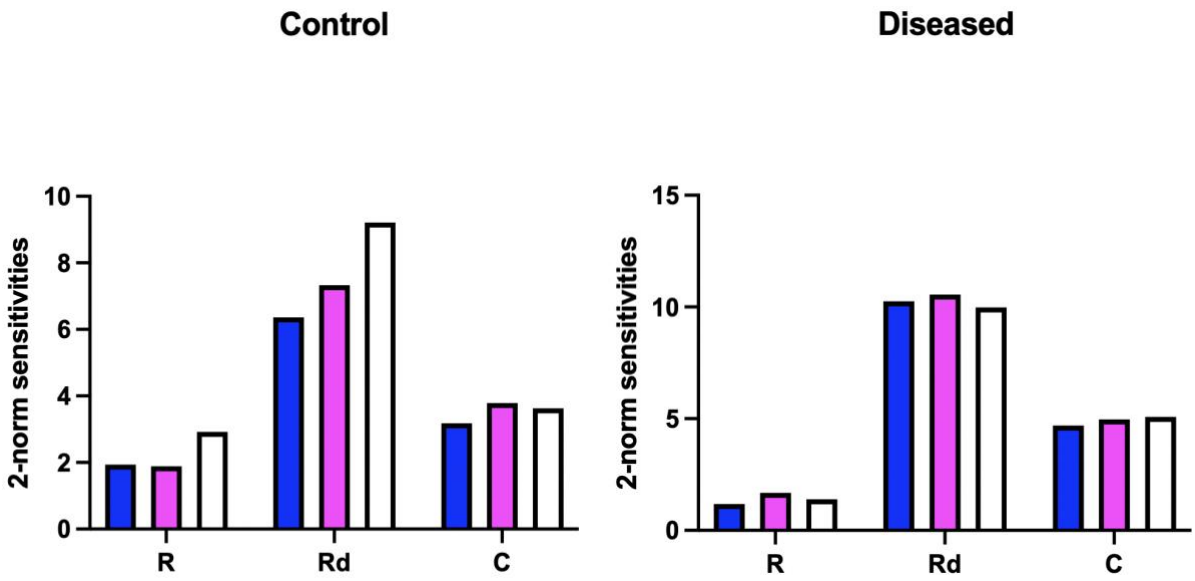

Figure 3.7: (Top) Relative sensitivity analysis of the three-element Windkessel model. (Bottom) 2-norm sensitivity magnitudes for the control and diseased (week 8) animals. The distal resistance parameter in all three groups of rats had the largest increase in relative sensitivity.

Table 3: Summary of the relative sensitivity ranking for male, female and OVX female at different stages of PAH. Distal Resistance (R_d) had the largest magnitude value and remained the most sensitive parameter to the model as PAH progresses over time in all three groups of rats.

	Control	Week-4	Week-8
Male	R: 1.94 Rd: 6.36 C: 3.18	R: 1.66 Rd: 10.37 C: 4.79	R: 1.18 Rd: 10.25 C: 4.69
Female	R: 1.89 Rd: 7.33 C: 3.79	R: 0.98 Rd: 12.39 C: 5.86	R: 1.68 Rd: 10.56 C: 4.97
OVX	R: 2.92 Rd: 9.21 C: 3.63 Rd* dominates!	R: 1.93 Rd: 7.72 C: 4.19 Rd* dominates!	R: 1.39 Rd: 9.98 C: 5.08 Rd* dominates!

3.4. The Model Output in Response to Controlling Each Parameter

In order to identify the changes in pressure waveform, we controlled all the parameters and only changed one at a time. Figure 3.8 shows the effect in pressure waveforms when only compliance, proximal resistance or distal resistance is changed at a time. Figure 3.9 shows the effect in pressure waveform when two Windkessel parameters are changed at a time. Week 4 optimized parameters were used for this analysis because week 4 and week 8 were statistically no different. When all the other parameters are controlled and only proximal resistance is changed, an elevated systolic pressure in male was observed. Contrary to the proximal resistance, when distal resistance was changed an elevated diastolic pressure was observed in all three groups of rats.

Lastly, when the compliance was changed, a sharp decrease in diastolic pressure in addition to the increase in systolic pressure is noticed in both male, females and ovariectomized female rats.

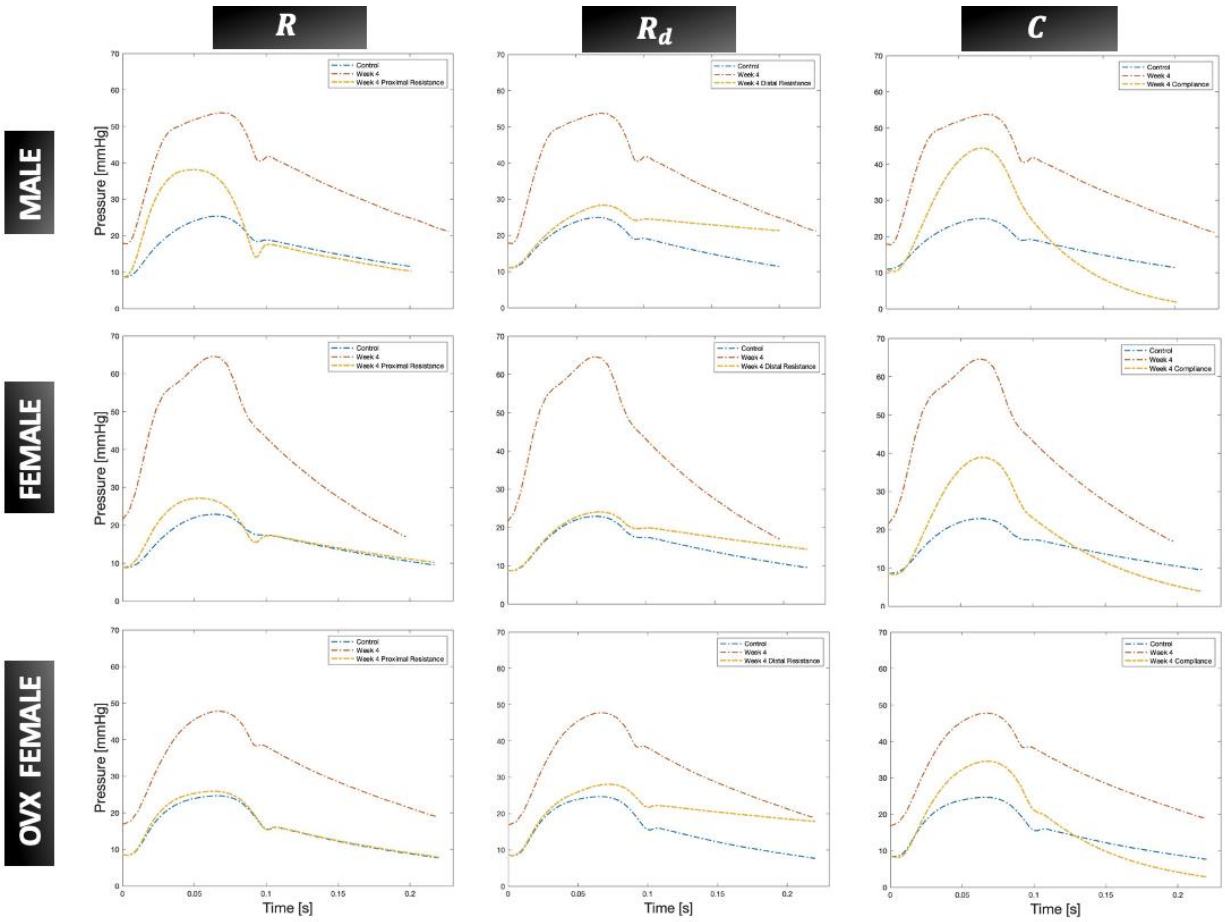

Figure 3.8: Pressure changes in male, female and ovariectomized female rats. The red curve indicates pressure waveform in week 4. The blue curve is the control. The yellow curve shows the pressure waveform when one optimized Windkessel parameter is changed at a time.

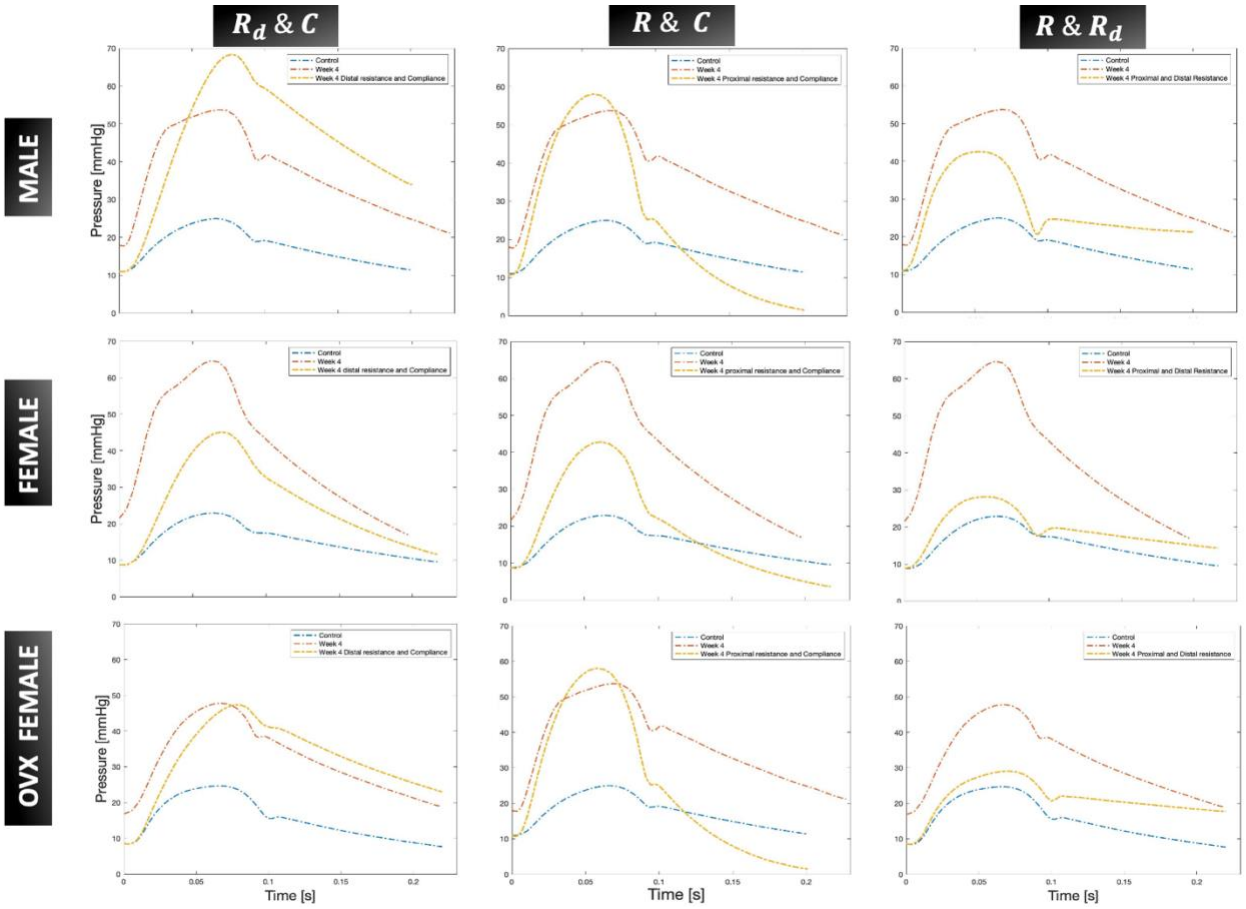

Figure 3.9: Pressure changes in male, female and OVX female rats when two Windkessel parameters are changed at a time. Changing distal resistance and compliance affects both the systolic and diastolic pressure changes in all three different groups of rats.

4. Discussion

As blood pressure increases, the resistance and compliance properties of the pulmonary vessel's changes. In this section, we analyze the relationship between these parameters estimated by the three- element Windkessel model and understand the sex-specific remodeling of pulmonary vasculature during PAH.

4.1. Pulmonary Vascular Properties

We investigated the changes in pulmonary vasculature properties as PAH progress in an animal model. We formulated and used a lumped three element Windkessel model to study the changes in resistance and compliance properties of a pulmonary vasculature during PAH. Our results revealed that, in addition to the pressure change, pulmonary vasculature properties significantly increase or decreases. A significant increase in both the proximal and distal resistance with an acute significant decrease in compliance was observed in males. However, in females only a significant decrease in compliance was noted. More importantly, the decrease in compliance occurred early on in the disease before any major changes in the resistance was observed. The decrease in compliance hence indicates stiffening of the vasculature as the resistance increases. These findings may be suggestive of an inverse relationship between the resistance and compliance properties of a pulmonary vasculature [9], [26], [44]. Additionally, the remodeling of pulmonary vasculature during PAH might be sex specific. Because, in females, PAH was mostly driven by the changes in compliance property but not the resistance. However, in males, changes in both the resistance and compliance properties were prominent. Also, no significant differences between the

female and OVX female rats were observed hence suggesting that the sex hormone– estrogen may not be regulating these changes in the pulmonary vasculature. However, further modeling effort needs to be done to understand sex-specific remodeling and the inverse relationship between the pulmonary vasculature properties as PAH progresses overtime.

Model Findings

4.2. Increase in the Pulmonary Arterial Pressure

Our results revealed that the mean pulmonary arterial pressure increases by a factor of 3 in all three groups of rats (male, female, OVX female) (Figure 3.4). More specifically, highest increase in the pressure was observed in diseased female rats at week 4. Additionally, by week 8, pressure seems to stabilize in female and OVX female rats but a slight insignificant increase in pressure was observed in diseased male rats. Although, difference in mPAP over the course of the disease were not significantly different across rats, sex specific remodeling of pulmonary vasculature existed. For instance, the increase in pressure in males during PAH was driven by the significant changes in both resistance and compliance properties. However, only the significant changes in compliance were observed in females. This might suggest that despite a pronounced increase in pressure, female rats have better prognosis with higher survival rate than males during PAH [36]. Unlike males, only the changes in compliance drives PAH in females and maybe physiologically females are more adaptive of the compliance changes than males. Moreover, further studies need to be done to understand the differences in the vasculature remodeling between male and female that causes an increase in pressure during PAH.

4.3. Changes in the Resistance and Compliance Parameters

Studies have shown that remodeling of pulmonary blood vessels, contributes to the elevated pulmonary vascular resistance (PVR), which is an important parameter used to clinically diagnose PAH [37]–[40]. In patients with PAH, early abnormalities in the pulmonary arteries characterized by vasoconstriction, increased medial thickness with plexiform-like lesion down the precapillary arterioles is observed which causes an increase in PVR [41]. Similarly, in SuHx animal model, increase in right ventricular systolic pressure (RVSP) was noted which is an indicator for an increase in the pulmonary vasculature remodeling during PAH [42], [43]. Because remodeling of pulmonary arteries is one of the many reasons for an elevated pulmonary arterial pressure, our model was used to predict the changes in the pulmonary vascular properties represented by the resistance and compliance parameter. The three-element Windkessel model was successfully able to show the inverse relationship between the resistance and compliance properties of the pulmonary arteries. As both the resistances significantly increases, compliance significantly drops as PAH progresses (Figure 3.6). This finding was supported by many other studies where an exponential increase in both the proximal and distal resistance with a sharp linear decrease in the compliance was found [42], [44]. Similarly, clinical studies done by Lankhaar *et al.* and his colleague also demonstrated an inverse-hyperbolic relationship between PVR and pulmonary artery compliance in 1,009 patients with confirmed PAH [28].

This study shows that the changes in both PVR and compliance in combination contributes to the increase in RV afterload. More specifically, a small increase in PVR highly influences the compliance as it significantly by as early as week 4. Compliance is an important property of the pulmonary vasculature that takes into account the pulsatile component of the arterial load and affects both the systolic and diastolic pressure changes in the pulmonary arteries. The increase in

systolic pressure determines the true afterload felt by the RV while the decrease in diastolic pressure represents the pulsatile component of the arterial load influenced by the elastic properties of the pulmonary circulation as it stiffens during the progression of PAH (Figure 3.8). For instance, the highest increase in systolic and diastolic pressure in all three groups of rats were observed when distal resistances and compliance was changed at a time. However, when both the proximal and distal resistances were changed, not much of an increase or decrease in the pressure waveforms were noted (Figure 3.9). This shows the contribution of compliance and the distal resistances in changing the pressure waveforms in different sexes of animals during PAH. Also, while computing the sensitivity analysis, both R_d and C parameter had the highest numerical ranking and similar magnitude values which remained unaffected as PAH progresses overtime (Figure 3.7). Hence, at a given flow, changes in compliance occurs at a very early stage of PAH before any major changes in the resistance is observed and that the rate at which the compliance decreases is not proportional to the rate at which resistance increases in any sexes of pulmonary hypertensive rats.

4.4. Sex-Specific Pulmonary Vasculature Remodeling During PAH

PAH is a severe disease that affects females 2-4 times more often than males [16]–[18]. In this study, we used three different groups of rats – male, female and OVX female- with an attempt to identify the sex specific remodeling of pulmonary vasculature during the progression of PAH. Figure 3.6 clearly shows the difference in the resistance and compliance properties of a pulmonary vasculature during PAH in different groups of rats. In females, only a significant change in the compliance was observed. Significant changes in both the resistances and compliance were observed in males. This could suggest that the origin and progression of PAH in females is highly dominated by the changes in the compliance parameter and not the resistance. However, unlike

females, changes in both the resistance and compliance parameters drives PAH in males. Because of these significantly greater changes in both the pulmonary vasculature properties in males, they tend to survive shorter than affected females. Affected females however have a better response to treatment with higher survival rates than males [45]–[47] . Moreover, several studies have also reported the importance of studying female sex hormone – estrogen- that might be attenuating the progression and severity of PAH in females.

Difference in sex during PAH has been described as “estrogen paradox”. From our model, no significant differences in the pulmonary vasculature properties and the pressures were observed in females and OVX female rats. However, studies have identified the sex steroids, 17β-estradiol (E2), that mediates the pro contractile, anti-inflammatory, and anti-apoptotic effects on RV which significantly improves the RV functionality without affecting any of the vascular remodeling during PAH [45]. For instance, Cheng *et al.* in his recent publication compared the mutant ERα receptor in both male and female rats where the male, but not female, were found to develop early RV fibrosis and diastolic dysfunction with plexiform like lesions in pulmonary arteries [48].

Moreover, with the E2 administration in these animals were shown to have a positive effect as it prevents RV dysfunction and increases the pulmonary arterial compliance by upregulating the enzymes such as ADAM17, ADAM15, osteopontin and apelin found in RV [45], [48]. Therefore, estrogen plays a key role in regulating the pressure and the vascular changes in the pulmonary arteries that must be further studied and examined to better understand the sex differences in PAH.

4.5. Limitations and Future Directions

The three-element Windkessel model is limited because it is a lumped model, and it neglects the wave transmission property in larger vessels. Using a lumped three-element

Windkessel model, we were not only able to estimate the changes in the resistance and compliance properties of a pulmonary vasculature but also show the dicrotic notch in the pressure waveform as the wave reflection property. However, as PAH progresses, the wave reflection intensity in addition to the vascular stiffness increases. Thus, a more advanced and robust models (one-dimensional fluid model) is required to accurately capture the changes in the resistance and compliance properties as pulmonary vasculature remodels during PAH. Future modeling effort should incorporate spatial representation of the pulmonary arterial system and show the overall contribution of wave propagation and reflection as PAH progresses in the animal models.

Furthermore, future work should compare the changes in structural and tissue-level biomechanical properties in the pulmonary arteries of male, female and OVX female rats. This could be done by using a tubular biaxial testing. Lastly, identifying the role of smooth muscle cells, endothelial cells and fibroblasts in pulmonary vasculature remodeling would potentially help improve our understanding of drug actions in either sex of PAH patients in future.

5. References

[1] W. C. Kwan, D. M. Shavelle, and D. R. Laughrun, “Pulmonary vascular resistance index: Getting the units right and why it matters,” *Clinical Cardiology*, vol. 42, no. 3. 2019. doi: 10.1002/clc.23151.

[2] V. V. McLaughlin, A. Shillington, and S. Rich, “Survival in primary pulmonary hypertension: The impact of epoprostenol therapy,” *Circulation*, vol. 106, no. 12, 2002, doi: 10.1161/01.CIR.0000029100.82385.58.

[3] T. Thenappan, M. L. Ormiston, J. J. Ryan, and S. L. Archer, “Pulmonary arterial hypertension: Pathogenesis and clinical management,” *BMJ (Online)*, vol. 360. 2018. doi: 10.1136/bmj.j5492.

[4] A. L. Firth, J. Mandel, and J. X. J. Yuan, “Idiopathic pulmonary arterial hypertension,” *DMM Disease Models and Mechanisms*, vol. 3, no. 5–6, 2010, doi: 10.1242/dmm.003616.

[5] N. F. Voelkel, J. Gomez-Arroyo, A. Abbate, H. J. Bogaard, and M. R. Nicolls, “Pathobiology of pulmonary arterial hypertension and right ventricular failure,” *European Respiratory Journal*, vol. 40, no. 6. 2012. doi: 10.1183/09031936.00046612.

[6] J. Deng, “Clinical application of pulmonary vascular resistance in patients with pulmonary arterial hypertension,” *Journal of Cardiothoracic Surgery*, vol. 16, no. 1. 2021. doi: 10.1186/s13019-021-01696-4.

[7] J. Widrich and M. Shetty, *Physiology, Pulmonary Vascular Resistance*. 2021.

[8] D. Akaslan *et al.*, “Change in pulmonary arterial compliance and pulmonary pulsatile stress after balloon pulmonary angioplasty,” *Anatol J Cardiol*, vol. 26, no. 1, 2022, doi: 10.5152/AnatolJCardiol.2021.149.

[9] J. W. Gerringer, J. C. Wagner, D. Vélez-Rendón, and D. Valdez-Jasso, “Lumped-parameter models of the pulmonary vasculature during the progression of pulmonary arterial hypertension,” *Physiol Rep*, vol. 6, no. 3, 2018, doi: 10.14814/phy2.13586.

[10] A. Giacomelli, “Integration of GIS and simulation models,” in *GIS for Sustainable Development*, 2005. doi: 10.1201/9781420037845.ch11.

[11] E. R. Pursell, D. Vélez-Rendón, and D. Valdez-Jasso, “Biaxial Properties of the Left and Right Pulmonary Arteries in a Monocrotaline Rat Animal Model of Pulmonary Arterial Hypertension,” *J Biomech Eng*, vol. 138, no. 11, 2016, doi: 10.1115/1.4034826.

[12] B. W. Christman *et al.*, "An Imbalance between the Excretion of Thromboxane and Prostacyclin Metabolites in Pulmonary Hypertension," *New England Journal of Medicine*, vol. 327, no. 2, 1992, doi: 10.1056/nejm199207093270202.

[13] O. Sitbon, L. Savale, X. Jaïs, D. Montani, M. Humbert, and G. Simonneau, "Treatment of pulmonary arterial hypertension," *Presse Medicale*, vol. 43, no. 9. 2014. doi: 10.1016/j.lpm.2014.07.011.

[14] A. Giaid, D. Saleh, M. Yanagisawa, and R. D. Clarke Forbes, "Endothelin-1 immunoreactivity and mRNA in the transplanted human heart," *Transplantation*, vol. 59, no. 9, 1995, doi: 10.1097/00007890-199505000-00015.

[15] H. C. Champion *et al.*, "Gene Transfer of Endothelial Nitric Oxide Synthase to the Lung of the Mouse In Vivo," *Circ Res*, vol. 84, no. 12, 1999, doi: 10.1161/01.res.84.12.1422.

[16] A. Foderaro and C. E. Ventetuolo, "Pulmonary Arterial Hypertension and the Sex Hormone Paradox," *Current Hypertension Reports*, vol. 18, no. 11. 2016. doi: 10.1007/s11906-016-0689-7.

[17] S. P. Gaine and L. J. Rubin, "Erratum: Primary pulmonary hypertension (The Lancet (1998) 29 August (723))," *Lancet*, vol. 353, no. 9146. 1999.

[18] Y. C. Lai, K. C. Potoka, H. C. Champion, A. L. Mora, and M. T. Gladwin, "Pulmonary arterial hypertension: The clinical syndrome," *Circ Res*, vol. 115, no. 1, 2014, doi: 10.1161/CIRCRESAHA.115.301146.

[19] K. Sagawa, R. K. Lie, and J. Schaefer, "Translation of Otto frank's paper 'Die Grundform des arteriellen Pulses' zeitschrift für biologie 37: 483-526 (1899)," *J Mol Cell Cardiol*, vol. 22, no. 3, 1990, doi: 10.1016/0022-2828(90)91459-K.

[20] N. Westerhof, G. Elzinga, and P. Sipkema, "An artificial arterial system for pumping hearts.," *J Appl Physiol*, vol. 31, no. 5, 1971, doi: 10.1152/jappl.1971.31.5.776.

[21] N. Westerhof, J. W. Lankhaar, and B. E. Westerhof, "The arterial windkessel," *Medical and Biological Engineering and Computing*, vol. 47, no. 2. 2009. doi: 10.1007/s11517-008-0359-2.

[22] R. Burattini, G. G. Knowlen, and K. B. Campbell, "Two arterial effective reflecting sites may appear as one to the heart," *Circ Res*, vol. 68, no. 1, 1991, doi: 10.1161/01.RES.68.1.85.

[23] M. F. O'Rourke, "Pressure and flow waves in systemic arteries and the anatomical design of the arterial system.," *J Appl Physiol*, vol. 23, no. 2, 1967, doi: 10.1152/jappl.1967.23.2.139.

[24] N. Stergiopulos, D. F. Young, and T. R. Rogge, "Computer simulation of arterial flow with applications to arterial and aortic stenoses," *J Biomech*, vol. 25, no. 12, 1992, doi: 10.1016/0021-9290(92)90060-E.

[25] A. Lungu, J. M. Wild, D. Capener, D. G. Kiely, A. J. Swift, and D. R. Hose, "MRI model-based non-invasive differential diagnosis in pulmonary hypertension," *J Biomech*, vol. 47, no. 12, 2014, doi: 10.1016/j.jbiomech.2014.07.024.

[26] T. Thenappan, K. W. Prins, M. R. Pritzker, J. Scandurra, K. Volmers, and E. K. Weir, "The critical role of pulmonary arterial compliance in pulmonary hypertension," *Annals of the American Thoracic Society*, vol. 13, no. 2. 2016. doi: 10.1513/AnnalsATS.201509-599FR.

[27] A. Lungu, D. R. Hose, D. G. Kiely, D. Capener, J. M. Wild, and A. J. Swift, "Three element windkessel model to non-invasively assess PAH patients: One year follow-up," in *IFMBE Proceedings*, 2017, vol. 59. doi: 10.1007/978-3-319-52875-5_34.

[28] J. W. Lankhaar *et al.*, "Quantification of right ventricular afterload in patients with and without pulmonary hypertension," *Am J Physiol Heart Circ Physiol*, vol. 291, no. 4, 2006, doi: 10.1152/ajpheart.00336.2006.

[29] L. A. Shimoda and S. S. Laurie, "Vascular remodeling in pulmonary hypertension," *Journal of Molecular Medicine*, vol. 91, no. 3. 2013. doi: 10.1007/s00109-013-0998-0.

[30] L. TARASEVICIENE-STEWART *et al.*, "Inhibition of the VEGF receptor 2 combined with chronic hypoxia causes cell death-dependent pulmonary endothelial cell proliferation and severe pulmonary hypertension," *The FASEB Journal*, vol. 15, no. 2, 2001, doi: 10.1096/fj.00-0343com.

[31] S. Sakao, K. Tatsumi, and N. F. Voelkel, "Endothelial cells and pulmonary arterial hypertension: Apoptosis, proliferation, interaction and transdifferentiation," *Respiratory Research*, vol. 10. 2009. doi: 10.1186/1465-9921-10-95.

[32] B. H. Freed *et al.*, "MR and CT Imaging for the Evaluation of Pulmonary Hypertension," *JACC: Cardiovascular Imaging*, vol. 9, no. 6. 2016. doi: 10.1016/j.jcmg.2015.12.015.

[33] F. Konecny, "Tools & Techniques for Pressure-Volume Hemodynamic Studies," 2019.

[34] F. Konecny, A. Haegens, C. McLarty, D. Senador, and M. Sosa, *The Guide to Acute Pressure and Flow Measurements in Rodents*. Cornelis J. Drost, 2019.

[35] M. Olufsen and A. Nadim, "On deriving lumped models for blood flow and pressure in the systemic arteries," *Mathematical Biosciences and Engineering*, vol. 1, no. 1, 2004, doi: 10.3934/mbe.2004.1.61.

[36] T. Lahm, "Sex differences in pulmonary hypertension: Are we cleaning up the mess?," *European Respiratory Journal*, vol. 47, no. 2. 2016. doi: 10.1183/13993003.01999-2015.

[37] R. J. Barst *et al.*, "Sitaxsentan Therapy for Pulmonary Arterial Hypertension," *Am. J. Respir. Crit. Care Med.*, vol. 169, no. 4, 2004, doi: 10.1164/rccm.200307-957oc.

[38] R. N. Channick *et al.*, "Effects of the dual endothelin-receptor antagonist bosentan in patients with pulmonary hypertension: A randomised placebo-controlled study," *Lancet*,

vol. 358, no. 9288, 2001, doi: 10.1016/S0140-6736(01)06250-X.

[39] X. Jaïs *et al.*, "Bosentan for Treatment of Inoperable Chronic Thromboembolic Pulmonary Hypertension. BENEFiT (Bosentan Effects in iNopErable Forms of chronIc Thromboembolic pulmonary hypertension), a Randomized, Placebo-Controlled Trial," *J. Am. Coll. Cardiol.*, vol. 52, no. 25, 2008, doi: 10.1016/j.jacc.2008.08.059.

[40] R. Voswinckel *et al.*, "Favorable Effects of Inhaled Treprostinil in Severe Pulmonary Hypertension. Results From Randomized Controlled Pilot Studies," *J. Am. Coll. Cardiol.*, vol. 48, no. 8, 2006, doi: 10.1016/j.jacc.2006.06.062.

[41] L. A. Shimoda and S. S. Laurie, "Vascular remodeling in pulmonary hypertension," *Journal of Molecular Medicine*, vol. 91, no. 3. 2013. doi: 10.1007/s00109-013-0998-0.

[42] M. A. De Raaf *et al.*, "SuHx rat model: Partly reversible pulmonary hypertension and progressive intima obstruction," *Eur. Respir. J.*, vol. 44, no. 1, 2014, doi: 10.1183/09031936.00204813.

[43] M. Zemskova *et al.*, "Necrosis-Released HMGB1 (High Mobility Group Box 1) in the Progressive Pulmonary Arterial Hypertension Associated with Male Sex," *Hypertension*, 2020, doi: 10.1161/HYPERTENSIONAHA.120.16118.

[44] D. Chemla, E. M. T. Lau, Y. Papelier, P. Attal, and P. Hervé, "Pulmonary vascular resistance and compliance relationship in pulmonary hypertension," in *European Respiratory Journal*, 2015, vol. 46, no. 4. doi: 10.1183/13993003.00741-2015.

[45] J. J. Rodriguez-Arias and A. García-Álvarez, "Sex Differences in Pulmonary Hypertension," *Front. Aging*, vol. 2, 2021, doi: 10.3389/fragi.2021.727558.

[46] K. Kozu *et al.*, "Sex differences in hemodynamic responses and long-term survival to optimal medical therapy in patients with pulmonary arterial hypertension," *Heart Vessels*, vol. 33, no. 8, 2018, doi: 10.1007/s00380-018-1140-6.

[47] T. Thenappan and E. Kenneth Weir, "Pulmonary arterial hypertension and sex in the right ventricle: It is an interesting picture!," *American Journal of Respiratory and Critical Care Medicine*, vol. 202, no. 7. 2020. doi: 10.1164/rccm.202006-2147ED.

[48] T. C. Cheng *et al.*, "Estrogen receptor-a prevents right ventricular diastolic dysfunction and fibrosis in female rats," *Am. J. Physiol. - Hear. Circ. Physiol.*, vol. 319, no. 6, 2020, doi: 10.1152/AJPHEART.00247.2020.